Modeling the Impact of Intentional Behavior in Supercomputing Environments via 1-D and 2-D Stochastic Fluid Queues Fed by an ON-OFF Source

by

Ning Liu

A thesis submitted to The Johns Hopkins University in conformity with the requirements for the degree of Master of Science.

Baltimore, Maryland

January, 2018

Abstract

High performance computers (HPCs) are being used within a wide range of academic, commercial, and governmental applications. However, the resilience of these systems is in question making them especially vulnerable to various forms of questionable activity. Our work explores modeling these intentional actions as a first-order stochastic fluid queue (SFQ) fed by an ON-OFF source. Here, the constant flow rates depict failures, resulting from the intentional actions, and the source represents the failure injections as a result of the users' actions. By performing spectral analysis techniques, the key contributions of this work are two-fold. First, closed-form solutions are derived depicting the probabilistic actions. Second, the transient analysis illustrates that the stability of the behavior depends on the combination of the flow rates, the state transition rates, and the Fourier modes. Numerical examples are provided which show that the proposed approach offers more granularity than prior works in SFQs that employ transform techniques. The results of this work can be leveraged to develop advanced frameworks for detection, analysis, and monitoring of Distributed Denial of Service (DDoS) attacks within supercomputing environments.

ABSTRACT

Research Advisor: Dr. Antwan Clark

Primary Reader: Prof. Minh Tang

Acknowledgments

I would like to acknowledge my research advisor, Dr. Antwan Clark for introducing me to the world of research, for guiding and encouraging me to write the thesis. His enthusiasm inspires me, and his kindness elevates me. He has taught me how to become a rigorous and independent researcher. It has been a truly incredible experience to learn from someone who is so passionate about the pursuit of new knowledge and teaching others.

I would like to thank Prof. Donniell Fishkind and Prof. Minh Tang, for their commitment to my personal and intellectual growth throughout my time at the Johns Hopkins University as well.

Lastly, I would like to thank my family and friends for their love, support and faith in me.

This work is based upon work supported by the U.S. Army Research Laboratory (ARL) and the U.S. Department of Defense under award numbers W911NF-13-D-0006 and 90074237 - FA8075-14-D-0002-0007, respectively. The views and conclusions contained in this document are those of the author and should not be interpreted as

necessarily representing the official policies, either expressed or implied, of the U.S. Army Research Laboratory or of the U. S. Department of Defense.

Contents

List of Tables

List of Figures

Chapter 1

Introduction

1.1 Motivation

High-performance computing systems (HPCs) use of supercomputers and parallel processing techniques to solve complex computational problems [2]. As a result, HPCs have accelerated technical developments in several areas such as modeling and simulation of scientific phenomenon as well as defense-related applications [3]. Although the development and deployment of these systems is steadily increasing, with the first U.S. exascale supercomputer anticipated to arrive circa 2023 [4], their reliability is expected to decrease [5]. This is because todays HPCs contain thousands of nodes representing multiple processors, which will statistically fail at some point [6]. These failures will not only impact operations, but will also be difficult to troubleshoot because of their complex infrastructure. These same factors also make these sys-

tems difficult to detect failures resulting from questionable activity. Hence, we need sophisticated processes to ensure systems resiliency against such behavior.

Resilience is defined as the the ability of a system to continue operation despite the presence of faults associated with it [7]. Thus, the primary goal is to ensure that HPCs continue running within some performance threshold when one or more system failures occur. Threat level behavior, which is in the realm of targeted failures, alludes to cyber-activity affecting overall system performance [8]. Therefore, these systems are also exposed to this type of activity. Furthermore, failures resulting from intentional actions are not necessarily related to the system failure rate, which are inversely proportional to the mean time between failures. The attacker can develop algorithms that first introduce unnoticeable failures then later inject high failures to cause serious harm. Conversely, malevolent algorithms can be created to inject steep numbers of failures, which can switch their course of action to operate at imperceptible rates while preparing subsequent moves. From the perspective of HPC managers, the difficulties are two-fold. Resuming operations of HPCs could prove detrimental because the attacker could continue to perform subsequent actions that cause additional harm. Additionally, we must give careful consideration prior to organizing a system shutdown of a cluster due to extensive preparation and planning [9].

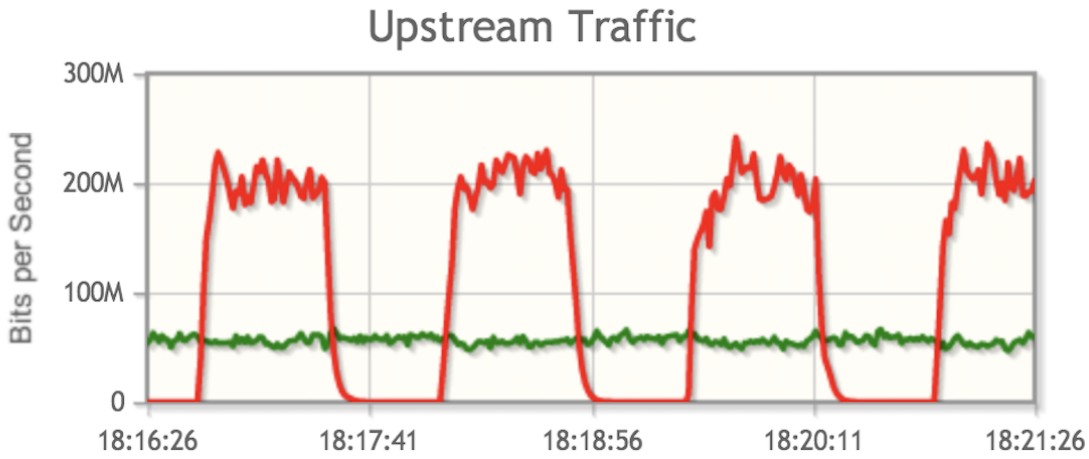

Figure 1.1: Example simulation of attack traffic (red) mixed with normal traffic (green) arriving at the edge switch [1].

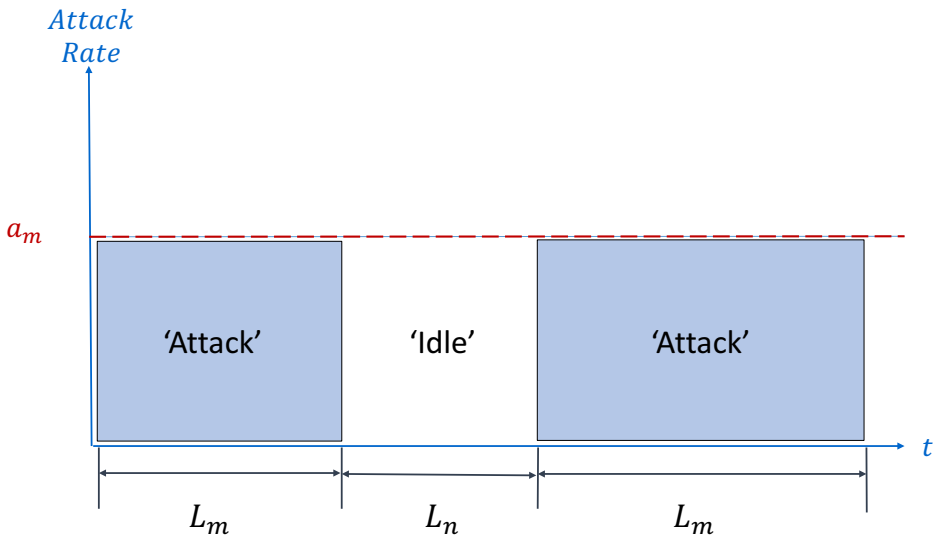

Figure 1.2: Pictorial representation of Figure 1.1. The CE attacks at a rate of a_m. During the idle attack periods, the server processes the information at a rate of a_n (not shown).

1.2 Related Work

Investigating resilience in distributed systems has spanned over the past six decades beginning with Von Neumann [10] who analyzed the effects of physical redundancy usage for reliable system performance. However, Gray revolutionized this area by revisiting Von Neumann's work and incorporated modular construction. As a result, his analysis significantly improved the redundancy factor as well as provided a systematic breakdown on failure causes [11]. He later revisited his work and discovered that software was the primary cause of system failures [12]. Gray's results stimulated investigations to understand the causes of failures within several systems including networks of workstations [13], enterprise-class server environments [14], network and internet systems [15], and HPCs [16]. These investigations provided no universal verdict as to how failures originate; however, conflicting viewpoints arose when studies were held using similar systems. For example, analysis on workstation networks illustrated juxtaposing viewpoints between software [13] and operator-related [17] causes of failures. These paradoxical perspectives were based on both the type of analyses and the data collected within a particular time frame.

Understanding targeted behavior in distributed systems has mainly been done from the perspective of malicious viruses in computer networks. Adopting mathematical epidemiological models, researchers have adopted equivalent models to describe virus propagation in computer networks. Motivated by the works of Kermack and McKendric (see [18–20]), Newmann *et al.* [21] developed analytical models to describe

viral behavior in email networks. Susceptible-infectious-susceptible (SIS) models were also adopted to investigate malicious behavior in computer networks [22]. Additionally, endemic models were used to analyze the effects of worm propagation. Using susceptible-exposed-infectious-susceptible with vaccination (SEIS-V) models, Mishra and Pandey performed stability analysis centering on the reproductive behavior of infected nodes [23]. Similarly, Zhang *et al* [24] explored the impact of virus-free periodic solutions for worm propagation. Investigations in worm propagation has also been explored in Facebook and email [25], mobile communication networks [26], and peer-to-peer communications [27].

On the other hand, understanding targeted failures in large scale parallel systems is a recent phenomenon. Inspired by game theoretic approaches [28], Faissol and Gallagher [29] examined the impact of variegated threatening behavior via considering the actions of malicious and selfish users. In this context, selfish users are those who are only concerned about their own self-interest instead of directly causing harm to the system [30]. Their approach showed potential in terms of characterizing detection ability, cost of attacks and repairs, and system characteristics. Later, Clark theoretically modeled the impact of targeted behavior to different risk levels [31]. In his analysis, he explored various components of failures and their impact from a probabilistic perspective where he also considered stopping considerations. Meanwhile, Pritchett-Sheats employed the conditional maximum likelihood estimator (CMLE) to perform automatic dynamic prediction of observed failure rates, which showed

promise for small configurations [32]. Motivated by this, Clark *et al.* [8] introduced a framework for improved prediction of observed failure rates consisting of a concatenation of data network extrapolation (DNE) and dynamic prediction processes. Their process outperformed that of Pritchett-Sheats [32] in terms of early prediction and accurate forecasting. Later, Clark and Absher [8] via adding a static characterization schema to their process, where their results showed a success rate of 70% in terms of failure spectrum characterization.

Transient analyses of stochastic fluid queues models have been explored by many authors [33–36]. However, the solutions are either based on recurrence relations [36] or expressed interms of Laplace transform and inverted numerically [33–35]. Exact solutions could not be obtained due to the complexity of the problem. Such solutions are useful in gaining insights and for comparing the relative merits of different numerical techniques. For example, in Parthasarathy and Vijayashree's work [37], the authors use double Laplace transform to obtain the transient solution of a simple fluid queue driven by an ON-OFF source with initial and boundary conditions in terms of modified Bessel's function of the first kind.

1.3 Approach

This work is extends that of Clark [31] via further analyzing the case of dynamic switching threat level behavior in HPCs. Here, we make the supposition that the

cyber enemy (CE) performs switching attacks, at either lower or higher failure rates, within each node of the supercomputing infrastructure. Hence, for any two consecutive threat levels we describe this behavior as a stochastic fluid queue fed by an ON-OFF source where each threat level is governed by constant virulent activity. Stochastic fluid queues have been studied extensively for many applications such as performance measurement of network switches [38]; peer-to-peer file sharing [39]; and analyzing battery life behavior [40]. However, the use of these models for understanding cyber behavior within HPCs is a novel exploration.

The major contributions in this work are three-fold. First, for the one-dimensional (1-D) case, we conducted transient analyses where we find closed-form solutions and stability criterion. This criterion considers the stability of the solutions due to the system failure rates, cyber attack rates, and Fourier modes. Next, our analyses is extended to the two-dimensional (2-D) case. However, in addition to the aforementioned criteria, the stability criterion also includes the application rates. Finally, for the 2-D case, we performed stationary analyses based on the relationship between the application rates and attack rates.

Chapter 2

Analysis of the 1-D Stochastic Fluid Queue (SFQ)

Our work explores the probabilistic impacts of virulent behavior within HPC infrastructures, via theorizing the influences of threat-level activity. Here, we assume that, for any node, the malicious behavior is governed via the piecewise differential equation

$$\frac{dx}{dt} = \begin{cases} a_m, \text{ if } x \in L_m \\ a_n, \text{ if } x \in L_n, \end{cases} \tag{2.1}$$

where a_m, $a_n \in \mathbb{R}^+$ are the constant cyber failure rates, $x \in \mathbb{R}^+$ is the total number of failed jobs, and the failure rate is defined as

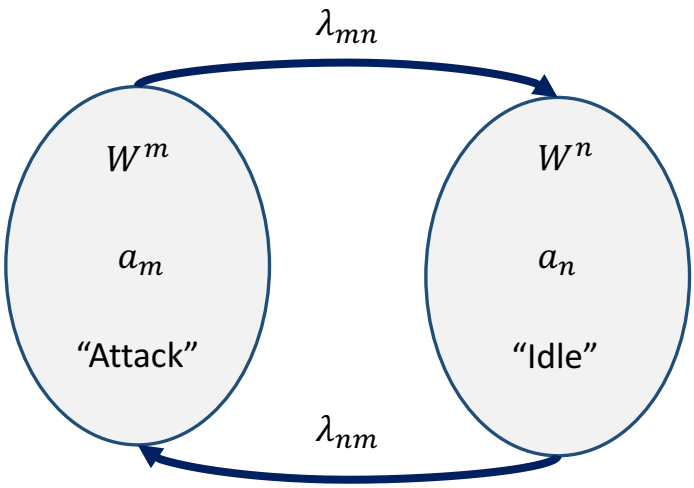

Figure 2.1: Illustration of the proposed Markovian process.

$$\frac{dx}{dt} = \frac{\text{total number of failed jobs}}{\text{time differential between failed jobs}}. \tag{2.2}$$

The threat levels L_m and L_n are subsets of $\mathbb{R}^+$ such that $L_m \cap L_n = \emptyset$. Therefore, we model the probabilistic effects as a stochastic fluid queue fed by an ON-OFF source. Our goal of the theoretical development is to understand the probabilistic cyber behavior within each threat level, we express threat level as following

$$W^m(x,t) = P\{x(t) = x | x \in L_m\}, \tag{2.3}$$

where x is the total number of failed jobs resulting from the cyber-activity, L_m is the

associated threat level, and $x(t)$ is the dynamic cyber behavior governed by equation (2.1). Hence, the stochastic behavior between two risk levels L_m and L_n is described as [37]

$$\begin{aligned} W_t^m &= -a_m W_x^m + (\lambda_{mn} W^n - \lambda_{nm} W^m) \\ W_t^n &= -a_n W_x^n + (\lambda_{nm} W^m - \lambda_{mn} W^n), \end{aligned} \tag{2.4}$$

where a_m and a_n are the corresponding cyber attack rates while λ_{mn} and λ_{nm} are the transition rates representing the system failure rate. Equation (2.4) describes the likelihood of the virulent activity reaching L_m and L_n while the system failure rate is also impacted. Additionally, by conducting intial detection of malicious activity, we describe the intial conditions as

$$W^m(x,0) = f(x) \qquad \text{and} \qquad W^n(x,0) = g(x). \tag{2.5}$$

We can represent the solution to the equation (2.4) by the complex Fourier series

$$W^m(x,t) = \sum_{-\infty}^{+\infty} A_k^m e^{jkx+ct} \tag{2.6}$$

and

$$W^n(x,t) = \sum_{-\infty}^{+\infty} A_k^n e^{jkx+ct}, \tag{2.7}$$

where $j = \sqrt{-1}$ and k is the Fourier mode number. Substituting into equation (2.4) we get the eigenvalue relationship for each mode

$$\mathcal{M}_k \boldsymbol{A_k} = c\boldsymbol{A_k}, \tag{2.8}$$

where $\boldsymbol{A_k} = [A_k^m, A_k^m]^T$ and

$$\mathcal{M}_k = \begin{bmatrix} -(\lambda_{nm} + jka_m) & \lambda_{mn} \\ \lambda_{nm} & -(\lambda_{mn} + jka_n) \end{bmatrix}. \tag{2.9}$$

For nontrivial solutions to exist, we need

$$c_{1,2} = -\frac{1}{2}\left[(\lambda_{mn} + \lambda_{nm}) + jk\left(a_m + a_n\right)\right] \pm \frac{1}{2}\sqrt{4\lambda_{mn}\lambda_{nm} + \left[jk\left(a_n - a_m\right) + (\lambda_{mn} - \lambda_{nm})\right]^2}. \tag{2.10}$$

To simplify the equation (2.10), we know that the radicand can be expressed as $\mathcal{R}e^{i\theta}$, where

$$\mathcal{R}(k) = \sqrt{\left[(\lambda_{nm} + \lambda_{mn})^2 - k^2(a_n - a_m)^2\right]^2 + 4k^2(a_n - a_m)^2(\lambda_{mn} - \lambda_{nm})^2} \tag{2.11}$$

and

$$\theta = tan^{-1}\left(\frac{2k(a_n - a_m)(\lambda_{mn} - \lambda_{nm})}{(\lambda_{nm} + \lambda_{mn})^2 - k^2(a_n - a_m)^2}\right). \tag{2.12}$$

Thus, equation(2.10) reduces to

$$c_{1,2} = -\frac{1}{2}\left[(\lambda_{mn} + \lambda_{nm}) + jk(a_m + a_n)\right] \pm \frac{1}{2}(\varphi_k + j\varpi_k) \tag{2.13}$$

where

$$\begin{aligned}
\varphi_k + j\varpi_k &= \sqrt{\mathcal{R}e^{j\theta}} \\
&= \sqrt{\mathcal{R}}e^{j\frac{\theta}{2}} \\
&= \sqrt{\mathcal{R}}cos\frac{\theta}{2} + j\sqrt{\mathcal{R}}sin\frac{\theta}{2} \\
&= \sqrt{\mathcal{R}}\sqrt{\frac{1 + cos\theta}{2}} + j\sqrt{\mathcal{R}}\sqrt{\frac{1 - cos\theta}{2}} \\
&= \sqrt{\frac{\mathcal{R} + \mathcal{R}cos\theta}{2}} + j\sqrt{\frac{\mathcal{R} - \mathcal{R}cos\theta}{2}},
\end{aligned} \tag{2.14}$$

Then we can express φ_k and ϖ_k respectively as

$$\varphi_k = \sqrt{\frac{\mathcal{R} + \mathcal{R}cos\theta}{2}} = \sqrt{\frac{\mathcal{R}(k) + (\lambda_{nm} + \lambda_{mn})^2 - k^2(a_n - a_m)^2}{2}} \tag{2.15}$$

and

$$\varpi_k = \sqrt{\frac{\mathcal{R} - \mathcal{R}cos\theta}{2}} = \sqrt{\frac{\mathcal{R}(k) - (\lambda_{nm} + \lambda_{mn})^2 + k^2(a_n - a_m)^2}{2}}. \tag{2.16}$$

Therefore, the general solutions are given by

$$W^m(x,t) = \sum_{-\infty}^{+\infty} \left(B_k e^{c_1(k)t} + C_k e^{c_2(k)t} \right) e^{jkx} \tag{2.17}$$

and

$$W^n(x,t) = \sum_{-\infty}^{+\infty} \left(B_k \xi_k e^{c_1(k)t} + C_k \chi_k e^{c_2(k)t} \right) e^{jkx}, \tag{2.18}$$

where ξ_k and χ_k are given by

$$\xi_k = \left(\frac{\lambda_{nm} - \lambda_{mn} + \varphi_k}{2\lambda_{mn}} \right) + j \left[\frac{k(a_m - a_n) + \varpi_k}{2\lambda_{mn}} \right] \tag{2.19}$$

and

$$\chi_k = \left(\frac{\lambda_{nm} - \lambda_{mn} - \varphi_k}{2\lambda_{mn}} \right) + j \left[\frac{k(a_m - a_n) - \varpi_k}{2\lambda_{mn}} \right]. \tag{2.20}$$

We employ the initial conditions (2.5) to achieve the exact solution for W^m and W^n, by calculating the coefficients B_k and C_k defined by the relationships

$$B_k = \alpha_k G(k) - \alpha_k \chi_k F(k) \tag{2.21}$$

and

$$C_k = (1 + \alpha_k \chi_k) F(k) - \alpha_k G(k)), \tag{2.22}$$

where $F(k)$ and $G(k)$ are given by

$$F(k) = \frac{1}{2\pi}\int_{-\pi}^{\pi} f(\zeta)e^{-jk\zeta}d\zeta \qquad \text{and} \qquad G(k) = \frac{1}{2\pi}\int_{-\pi}^{\pi} g(\zeta)e^{-jk\zeta}d\zeta \tag{2.23}$$

and α_k is described as

$$\alpha_k = \frac{1}{\xi_k - \chi_k} = \frac{\lambda_{mn}}{\varphi_k + j\varpi_k}. \tag{2.24}$$

It is important to note that cyber activity can still exist where the overall system response, otherwise known as the system failure rate, can appear unaffected. Thus, we need to consider Poisson transitions where $\lambda_{mn} = \lambda_{nm} = \lambda$. For this scenario, the solution for W^m and W^n is of the form expressed in equations (2.17) and (2.18), where

$$\xi_k, \chi_k = \frac{jk(a_m - a_n)}{2\lambda} \pm \sqrt{1 - \frac{k^2}{4\lambda^2}(a_n - a_m)^2}. \tag{2.25}$$

Similarly, we can abtain an exact solution from the initial conditions (2.5), by calculating the coefficients B_k and C_k from (2.21), (2.22) and (2.23) where α_k is given by

$$\alpha_k = \frac{\lambda}{\sqrt{4\lambda^2 - k^2(a_n - a_m)^2}}. \tag{2.26}$$

2.1 Transient Analysis

We perform transient analysis by way of understanding the stability of W^m and W^n, which means examining the eigenvalue spectrum $c(k) = c_r(k) + jc_j(k)$. When $c_r(k) > 0$, we get unstable solutions; however, a refined instability estimate is provided in the following theorem

Theorem 2.1.1. *The solutions W^m and W^n of the stochastic fluid queue (2.4) are unstable whenever the complex eigenvalue $c(k) = c_r(k)+jc_j(k)$ falls within the domain*

$$\begin{cases} \left(c_r(k) + \frac{\lambda_{mn}+\lambda_{nm}}{2}\right)^2 + \left(c_j(k) + k\frac{a_m+a_n}{2}\right)^2 \leq \frac{\mathcal{R}}{4}, \\ c_r(k) > 0 \end{cases} \tag{2.27}$$

where $\mathcal{R}$ is defined by (2.11).

Proof. Noting that the eigenvalue $c(k) = c_r(k) + jc_j(k)$, the exponential terms are expressed as

$$e^{jkx+c(k)t} = e^{c_r(k)t} \cdot e^{j(kx+c_j(k)t)}, \tag{2.28}$$

which shows that unstable solutions exist for $c_r(k) > 0$. Equation (2.14) can be written as

$$\left(c_r(k) + \frac{\lambda_{mn}+\lambda_{nm}}{2}\right) + j\left(c_j(k) + k\frac{a_m+a_n}{2}\right) = \pm\frac{1}{2}(\varphi_k + \varpi_k), \tag{2.29}$$

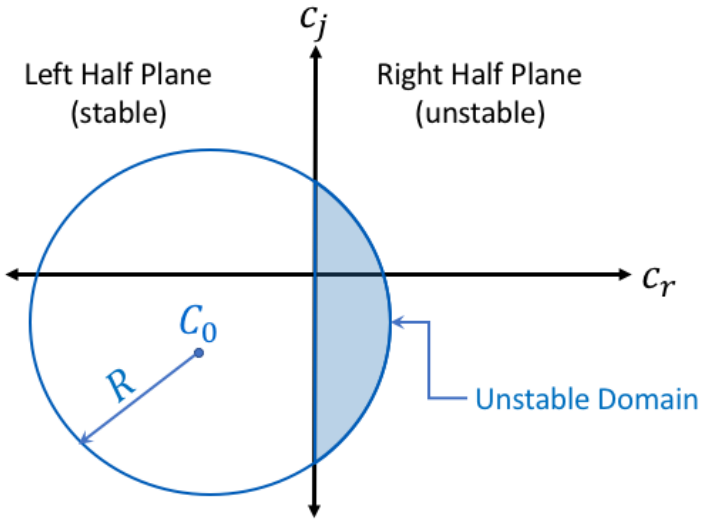

Figure 2.2: Pictorial representation of Theorem 2.1.1 in the complex plane with the shaded unstable domain. The circular portion of the domain is given by equation(2.30) with center $C_0 = (-\frac{\lambda_{mn}+\lambda_{nm}}{2}, -k\frac{a_m+a_n}{2})$

with φ_k and ϖ_k given by equations (2.15) and (2.16). Taking the squared norm on both sides of equation (2.29) yields

$$\left(c_r(k) + \frac{\lambda_{mn} + \lambda_{nm}}{2}\right)^2 + \left(c_j(k) + k\frac{a_m + a_n}{2}\right)^2 = \frac{\mathcal{R}(k)}{4}. \tag{2.30}$$

Instability occurs when, in the complex plane, equation (2.30) intersects with $c_r > 0$ producing the region (2.27). □

As Figure 2.2 illustrates, Theorem 2.1.1 directly shows the relationship between the cyber-attack rates, system failure rates, and Fourier modes. Once we know these unstable modes, we can find stable solutions. If we know the attack and transition rates, we can use Theorem 2.1.1 to estimate which modal solutions are unstable.

From this, an argument similar to the work of Parthasarathy and Vijayashree [37] can be applied such that the coefficient of each unstable Fourier mode B_k must equal zero to ensure stable solutions.

When malevolent actions don't change the system failure rates, $\lambda_{mn} = \lambda_{nm} = \lambda$ yielding the following result

Theorem 2.1.2. *Let $\lambda_{mn} = \lambda_{nm} = \lambda$, The solutions W^m and W^n of the stochastic fluid queue (2.4) are stable for any combination of attack rates a_m and a_n, system failure rate, and Fourier mode number k.*

Proof. When $\lambda_{mn} = \lambda_{nm} = \lambda$, the eigenvalue spectrum becomes

$$c_{1,2}(k) = -\lambda + jk\frac{a_m + a_n}{2} \pm \sqrt{\lambda^2 - k^2\left(\frac{a_n - a_m}{2}\right)^2}. \tag{2.31}$$

The following inequality

$$Re\left\{-\lambda + \sqrt{\lambda^2 - k^2\left(\frac{a_n - a_m}{2}\right)^2}\right\} \leq 0, \tag{2.32}$$

where Re denotes the real part, consistently holds producing stable solutions. □

Theorem 2.1.2 implies that when the overall system failure rate is unaffected by virulent activity, the solutions W^m and W^n will always be stable. Hence, the transient analysis for this case solely involves examining the probabilistic impacts of cyber behavior over time while considering various estimates for a_m, a_n, and λ. Here,

we can study the temporal behavior of W^m and W^n by examining the decay rate behavior as presented in the following corollary

Corollary 2.1.1. *For $\lambda_{mn} = \lambda_{nm} = \lambda$, the decay rate $c_r(k)$ converges to $-\lambda$ as*

$$k \to \pm \frac{2\lambda}{a_n - a_m} \tag{2.33}$$

for any combination of attack rates, a_m and a_n, and system failure rate λ.

Proof. This is done via examing the inequality

$$\lambda^2 - k^2(\frac{a_n - a_m}{2})^2 \leq 0, \tag{2.34}$$

which holds for $k \in (-\infty, -k_{cr}] \cup [k_{cr}, \infty)$ where

$$k_{cr} = \frac{2\lambda}{a_n - a_m}. \tag{2.35}$$

Therefore, from (2.31) $c_r(k) = Re\{c_{1,2}(k)\} = -\lambda$ □

2.2 Stationary Analysis

Not all cyber attacks are immediately detected. Therefore, it is also imperative to investigate the probabilistic effects of long-term malicious activity. Assuming stationary behavior, equation (2.4) reduces to the system

$$\begin{aligned} a_m \frac{\partial \Psi^m}{\partial x} &= (\lambda_{mn}\Psi^n - \lambda_{nm}\Psi^m) \\ a_n \frac{\partial \Psi^n}{\partial x} &= (\lambda_{nm}\Psi^m - \lambda_{mn}\Psi^n), \end{aligned} \tag{2.36}$$

where Ψ^m and Ψ^n are the stationary distributions corresponding to threat levels S_m and S_n, respectively. Since this is a ODE system only corresponding to x. We can solve the system by making the following assumption:

$$\Psi^{m,n} = \beta_{m,n}(x)e^{\gamma x}, \tag{2.37}$$

where γ represents the eigenvalues. For nontrivial solutions to exist, we require that

$$\gamma_1 = 0 \tag{2.38}$$

and

$$\gamma_2 = -\Big(\frac{\lambda_{nm}}{a_m} + \frac{\lambda_{mn}}{a_n}\Big). \tag{2.39}$$

Therefore, the general solution for $\Psi(x)$ can be described as

$$\Psi(x) = \begin{bmatrix} \Psi^m(x) \\ \\ \Psi^n(x) \end{bmatrix} = \beta_1(x) \begin{bmatrix} 1 \\ \\ \frac{\lambda_{nm}}{\lambda_{mn}} \end{bmatrix} + \beta_2(x) \begin{bmatrix} 1 \\ \\ -\frac{a_m}{a_n} \end{bmatrix} e^{\gamma x} \tag{2.40}$$

where

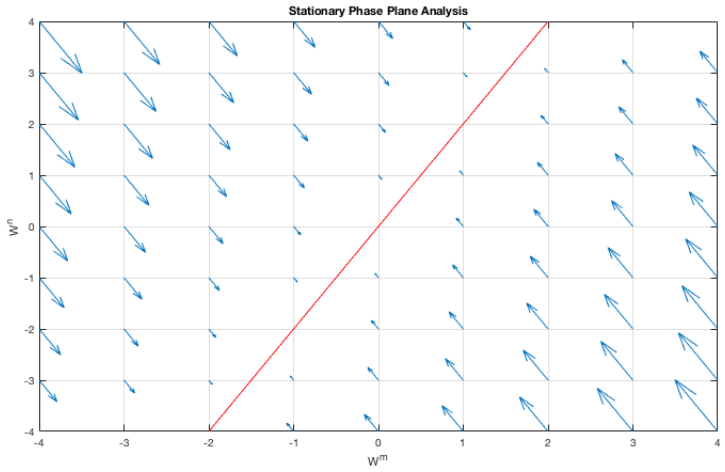

Figure 2.3: Phase plane portrait of (2.40) with $a_m = 2$, $a_n = 1$, $\lambda_{mn} = 1$ and $\lambda_{nm} = 2$. Notice the spectrum of solutions merging to the equilibrium line defined by the eigenvector $[1, 2]^T$.

$$\gamma = \gamma_2 = -\left(\frac{\lambda_{nm}}{a_m} + \frac{\lambda_{mn}}{a_n}\right) \tag{2.41}$$

Figure 2.3 is the phase plane representation, which shows stable behavior of (2.40) converging to the line defined by the eigenvector $[1, \lambda_{nm}/\lambda_{mn}]^T$. This line is known as the attractive line of equilibrium. This result shows that as the number of failed jobs x increases the stationary distributions solely depend on the affected system failure rates. Hence, it can be inferred that as the virulent behavior becomes more dominant the effects of the attack rates become insignificant. Intuitively, this makes sense because at this point the system will become severely infected. When $\lambda_{mn} = \lambda_{nm} = \lambda$, similar behavior is observed where the attractive line of equilibrium is governed by $[1, 1]^T$.

Chapter 3

Analysis of the 2-D Stochastic Fluid Queue (SFQ)

Now, we are exploring the 2-D Stochastic Fluid Queue case. We assume that, for any node, the malicious behavior is governed via the differential equations

$$\frac{dx}{dt} = \begin{cases} a_m, \text{ if } x \in L_m \\ a_n, \text{ if } x \in L_n \end{cases} \qquad \text{and} \qquad \frac{dy}{dt} = \begin{cases} r_m, \text{ if } y \in L_m \\ r_n, \text{ if } y \in L_n, \end{cases} \tag{3.1}$$

where a_m, $a_n \in \mathbb{R}^+$ are the constant cyber failure rates, r_m, $r_n \in \mathbb{R}^+$ are the constant cyber infected rates, $x \in \mathbb{R}^+$ is the total number of failed jobs, $y \in \mathbb{R}^+$ is the number of infected applications and the failure rate is defined as

$$\frac{dx}{dt} = \frac{\text{total number of failed jobs}}{\text{time differential between failed jobs}} \tag{3.2}$$

and

$$\frac{dy}{dt} = \frac{\text{total number of infected applications}}{\text{time differential between infected applications}}. \tag{3.3}$$

The threat levels L_m and L_n are subsets of $\mathbb{R}^+$ such that $L_m \cap L_n = \emptyset$. Therefore, we model the probabilistic effects as a 2-D stochastic fluid queue fed by an ON-OFF source. Our goal of the theoretical development is to understand the probabilistic cyber behavior within each threat level, we express threat level as following

$$W^m(x, y, t) = P\{x(t) = x, y(t) = y | x, y \in L_m\}, \tag{3.4}$$

where x is the total number of failed jobs resulting from the cyber-activity, y is the total number of infected applications resulting from the cyber-activity, L_m is the associated threat level, and $x(t)$ and $y(t)$ is the dynamic cyber behavior governed by equation (3.1). Hence, the stochastic behavior between two risk levels L_m and L_n is described as [41]

$$\begin{aligned} W_t^m &= -a_m W_x^m - r_m W_y^m + (\lambda_{mn} W^n - \lambda_{nm} W^m) \\ W_t^n &= -a_n W_x^n - r_n W_y^n + (\lambda_{nm} W^m - \lambda_{mn} W^n), \end{aligned} \tag{3.5}$$

where a_m and a_n are the corresponding cyber failure rates and r_m and r_n are the

corresponding cyber infected rates while λ_{mn} and λ_{nm} are the transition rates representing the system failure rate. Equation (3.5) describes the likelihood of the virulent activity reaching L_m and L_n as two stochastic fluid flows driven by the same Markow chain. Here the intial conditions now become

$$W^m(x, y, 0) = f(x, y) \qquad \text{and} \qquad W^n(x, y, 0) = g(x, y). \tag{3.6}$$

Similar to Chapter 2, we can represent the solution to the equation (3.5) by the complex Fourier series

$$W^m(x, y, t) = \sum_{k=-\infty}^{+\infty} \sum_{l=-\infty}^{+\infty} A^m_{k,l} e^{j(kx+ly)+ct} \tag{3.7}$$

and

$$W^n(x, y, t) = \sum_{k=-\infty}^{+\infty} \sum_{l=-\infty}^{+\infty} A^n_{k,l} e^{j(kx+ly)+ct}, \tag{3.8}$$

where $j = \sqrt{-1}$ and k and l are the Fourier mode numbers in the x and y directions. Substituting (3.7) and (3.8) into equations (3.5) we get the eigenvalue relationship for each mode

$$\mathcal{M}_{k,l} \boldsymbol{A_{k,l}} = c \boldsymbol{A_{k,l}}, \tag{3.9}$$

where $\boldsymbol{A_{k,l}} = [A^m_{k,l}, A^n_{k,l}]^T$ and

$$\mathcal{M}_{k,l} = \begin{bmatrix} -[\lambda_{nm} + j(ka_m + lr_m)] & \lambda_{mn} \\ \lambda_{nm} & -[\lambda_{mn} + j(ka_n + lr_n)] \end{bmatrix}. \tag{3.10}$$

For nontrivial solutions to exist, we need

$$\begin{aligned} c_{1,2} = &-\frac{1}{2}\left[(\lambda_{mn} + \lambda_{nm}) + jk(a_m + a_n) + jl(r_m + r_n)\right] \\ &\pm \frac{1}{2}\sqrt{4\lambda_{mn}\lambda_{nm} + \left[jk(a_n - a_m) + jl(r_n - r_m) + (\lambda_{mn} - \lambda_{nm})\right]^2}. \end{aligned} \tag{3.11}$$

Similar to equation(2.10), equation(3.11) reduces to

$$c_{1,2} = -\frac{1}{2}\left[(\lambda_{mn} + \lambda_{nm}) + jk(a_m + a_n) + jl(r_m + r_n)\right] \pm \frac{1}{2}(\varphi_{k,l} + j\varpi_{k,l}) \tag{3.12}$$

where $\varphi_{k,l}$ and $\varpi_{k,l}$ are given as

$$\varphi_{k,l} = \sqrt{\frac{\mathcal{R}(k,l) + (\lambda_{nm} + \lambda_{mn})^2 - k^2(a_n - a_m)^2 - l^2(r_n - r_m)^2}{2}} \tag{3.13}$$

and

$$\varpi_{k,l} = \sqrt{\frac{\mathcal{R}(k,l) - (\lambda_{nm} + \lambda_{mn})^2 + k^2(a_n - a_m)^2 + l^2(r_n - r_m)^2}{2}} \tag{3.14}$$

and $R(k,l)$ is defined as

$$\begin{aligned} R(k,l) = \Big\{ & \left[-k^2(a_n - a_m)^2 - l^2(r_n - r_m)^2 + (\lambda_{mn} + \lambda_{nm})^2\right]^2 \\ & + 4\left[k(a_n - a_m)(\lambda_{mn} - \lambda_{nm}) + l(r_n - r_m)(\lambda_{mn} - \lambda_{nm})\right]^2 \Big\}^{\frac{1}{2}} \end{aligned} \tag{3.15}$$

Therefore, the general solutions are given by

$$W^m(x,y,t) = \sum_{k=-\infty}^{+\infty} \sum_{l=-\infty}^{+\infty} \left(B_{k,l} e^{c_1(k,l)t} + C_{k,l} e^{c_2(k,l)t}\right) e^{j(kx+ly)} \tag{3.16}$$

and

$$W^n(x,y,t) = \sum_{k=-\infty}^{+\infty} \sum_{l=-\infty}^{+\infty} \left(B_{k,l}\xi_{k,l} e^{c_1(k,l)t} + C_{k,l}\chi_{k,l} e^{c_2(k,l)t}\right) e^{j(kx+ly)}, \tag{3.17}$$

where $\xi_{k,l}$ and $\chi_{k,l}$ are given by

$$\xi_{k,l} = \left(\frac{\lambda_{nm} - \lambda_{mn} + \varphi_{k,l}}{2\lambda_{mn}}\right) + j\left[\frac{k(a_m - a_n) + l(r_m - r_n) + \varpi_{k,l}}{2\lambda_{mn}}\right] \tag{3.18}$$

and

$$\chi_{k,l} = \left(\frac{\lambda_{nm} - \lambda_{mn} - \varphi_{k,l}}{2\lambda_{mn}} \right) + j \left[\frac{k(a_m - a_n) + l(r_m - r_n) - \varpi_{k,l}}{2\lambda_{mn}} \right]. \tag{3.19}$$

We employ the initial conditions (3.6) to achieve the exact solution for W^m and W^n, by calculating the coefficients $B_{k,l}$ and $C_{k,l}$ defined by the relationships

$$B_{k,l} = \alpha_{k,l} G(k,l) - \alpha_{k,l} \chi_{k,l} F(k,l) \tag{3.20}$$

and

$$C_{k,l} = (1 + \alpha_{k,l} \chi_{k,l}) F(k,l) - \alpha_{k,l} G(k,l)), \tag{3.21}$$

where $F(k,l)$ and $G(k,l)$ are given by

$$F(k,l) = \frac{1}{(2\pi)^2} \int_{-\pi}^{\pi} \int_{-\pi}^{\pi} f(\zeta,\eta) e^{-j(k\zeta + l\eta)} d\zeta d\eta \tag{3.22}$$

and

$$G(k,l) = \frac{1}{(2\pi)^2} \int_{-\pi}^{\pi} \int_{-\pi}^{\pi} g(\zeta,\eta) e^{-j(k\zeta + l\eta)} d\zeta d\eta \tag{3.23}$$

and $\alpha_{k,l}$ is described as

$$\alpha_{k,l} = \frac{1}{\xi_{k,l} - \chi_{k,l}} = \frac{\lambda_{mn}}{\varphi_{k,l} + j\varpi_{k,l}}. \tag{3.24}$$

If the cyber activity does not affect overall system, we need to consider Poisson transitions where $\lambda_{mn} = \lambda_{nm} = \lambda$. Thus, the solution for W^m and W^n is of the form expressed in equation (3.16) and (3.17) where

$$\xi_{k,l}, \chi_{k,l} = \frac{j\left[k(a_m - a_n) + l(r_m - r_n)\right]}{2\lambda} \pm \sqrt{1 - \frac{k^2}{4\lambda^2}\left[(a_n - a_m)^2 + (r_n - r_m)^2\right]} \tag{3.25}$$

Similarly, we can abtain an exact solution from the initial conditions (3.6), by calculating the coefficients $B_{k,l}$ and $C_{k,l}$ from (3.20), (3.21), (3.22) and (3.23) where $\alpha_{k,l}$ is given by

$$\alpha_{k,l} = \frac{\lambda}{\sqrt{4\lambda^2 - k^2(a_n - a_m)^2 - l^2(r_n - r_m)^2}} \tag{3.26}$$

3.1 Transient Analysis

Transient analysis is done by way of understanding the stability of W^m and W^n, which means examining the eigenvalue spectrum $c(k,l) = c_r(k,l) + jc_j(k,l)$. When $c_r(k,l) > 0$, we get unstable solutions; however, an analog to Theorem 2.1.1 is found, where a refined instability estimate is provided in the following theorem

Theorem 3.1.1. *The solutions W^m and W^n of the stochastic fluid queue (3.5) are unstable whenever the complex eigenvalue $c(k,l) = c_r(k,l) + jc_j(k,l)$ falls within the domain*

$$\begin{cases} \left(c_r(k,l) + \frac{\lambda_{mn}+\lambda_{nm}}{2}\right)^2 + \left(c_j(k,l) + k\frac{a_m+a_n}{2} + l\frac{r_m+r_n}{2}\right)^2 \leq \frac{\mathcal{R}}{4}, \\ c_r(k,l) > 0 \end{cases} \tag{3.27}$$

where $\mathcal{R}$ is defined by (3.15).

Proof. Noting that the eigenvalue $c(k,l) = c_r(k,l) + jc_j(k,l)$, the exponential terms are expressed as

$$e^{j(kx+ly)+c(k,l)t} = e^{c_r(k,l)t} \cdot e^{j(kx+ly+c_j(k,l)t)}, \tag{3.28}$$

which shows that unstable solutions exist for $c_r(k,l) > 0$. Equation (3.12) can be written as

$$\left(c_r(k,l) + \frac{\lambda_{mn}+\lambda_{nm}}{2}\right) + j\left(c_j(k,l) + k\frac{a_m+a_n}{2} + l\frac{r_m+r_n}{2}\right) = \pm\frac{1}{2}(\varphi_{k,l} + \varpi_{k,l}), \tag{3.29}$$

with $\varphi_{k,l}$ and $\varpi_{k,l}$ given by equations (3.13) and (3.14). Taking the squared norm on both sides of equation (3.29) yields

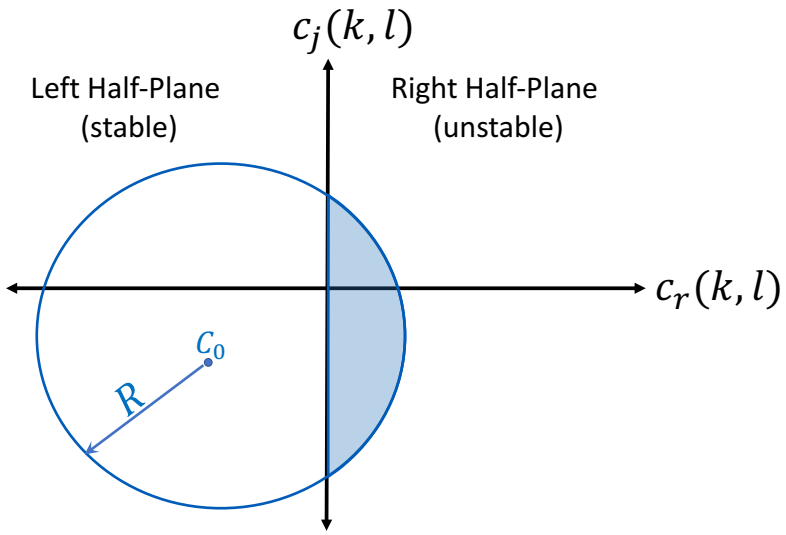

Figure 3.1: Pictorial representation of Theorem 3.1.1 in the complex plane with the shaded unstable domain. The circular portion of the domain is given by equation(3.30) with center $C_0 = (-\frac{\lambda_{mn}+\lambda_{nm}}{2}, -k\frac{a_m+a_n}{2} - l\frac{r_m+r_n}{2})$

$$\left(c_r(k,l) + \frac{\lambda_{mn}+\lambda_{nm}}{2}\right)^2 + \left(c_j(k,l) + k\frac{a_m+a_n}{2} + l\frac{r_m+r_n}{2}\right)^2 = \frac{\mathcal{R}(k,l)}{4}. \quad (3.30)$$

Instability occurs when, in the complex plane, equation (3.30) intersects with $c_r > 0$ producing the region (3.27). □

Similar to Theorem 2.1.1, Theorem 3.1.1 shows the relationship between the cyber-attack rates, system failure rates, and Fourier modes, as Figure 3.1 illustrates. Once we know these unstable modes, we can find stable solutions. If we know the attack and transition rates, we can use Theorem 3.1.1 to estimate which modal solutions are unstable. From this, an argument similar to [37] can be applied such that the coeffi-

cient of each unstable Fourier mode $B_{k,l}$ must equal zero to ensure stable solutions.

When malevolent actions don't change the system failure rates, $\lambda_{mn} = \lambda_{nm} = \lambda$ yielding the following result

Theorem 3.1.2. *Let $\lambda_{mn} = \lambda_{nm} = \lambda$, The solutions W_m and W_n of the stochastic fluid queue (3.5) are stable for any combination of attack rates a_m and a_n, system failure rate λ, and Fourier mode numbers k and l.*

Proof. When $\lambda_{mn} = \lambda_{nm} = \lambda$, the eigenvalue spectrum becomes

$$c_{1,2}(k,l) = -\lambda + j\left(k\frac{a_m + a_n}{2} + l\frac{r_m + r_n}{2}\right) \pm \sqrt{\lambda^2 - \left[k\left(\frac{a_n - a_m}{2}\right) + l\left(\frac{r_n - r_m}{2}\right)\right]^2}. \tag{3.31}$$

The following inequality

$$Re\left\{-\lambda + \sqrt{\lambda^2 - \left[k\left(\frac{a_n - a_m}{2}\right) + l\left(\frac{r_n - r_m}{2}\right)\right]^2}\right\} \leq 0, \tag{3.32}$$

where Re denotes the real part, consistently holds producing stable solutions. □

Theorem 3.1.2 implies that when the overall system failure rate is unaffected by virulent activity, the solutions W^m and W^n will always be stable. Hence, the transient analysis solely involves examining the probabilistic impacts of cyber behavior over time while considering various estimates for a_m, a_n, r_m, r_n and λ. In this case, we can study the temporal behavior of W^m and W^n by examining the decay rate behavior

as presented in the following corollary

Corollary 3.1.1. *For $\lambda_{mn} = \lambda_{nm} = \lambda$, the decay rate $c_r(k,l)$ converges to $-\lambda$ as*

$$[k(a_n - a_m) + l(r_n - r_m)] \to \pm 2\lambda \tag{3.33}$$

for any combination of attack rates, a_m and a_n, infected application rates r_m and r_n, and system failure rate λ.

Proof. This is done via examing the inequality

$$\lambda^2 - \left[k\left(\frac{a_n - a_m}{2}\right) + l\left(\frac{r_n - r_m}{2}\right)\right]^2 \leq 0, \tag{3.34}$$

then we have $[k(a_n - a_m) + l(r_n - r_m)] \in (-\infty, -2\lambda] \cup [2\lambda, +\infty)$. Therefore, from (3.31) $c_r(k,l) = Re\{c_{1,2}(k,l)\} = -\lambda$. □

3.2 Stationary Analysis

To understand the behavior of long-term questionable activity, we assume stationary behavior, where equation (3.5) reduces to the system

$$a_m \frac{\partial \Psi^m}{\partial x} + r_m \frac{\partial \Psi^m}{\partial y} = (\lambda_{mn}\Psi^n - \lambda_{nm}\Psi^m) \tag{3.35}$$

$$a_n \frac{\partial \Psi^n}{\partial x} + r_n \frac{\partial \Psi^n}{\partial y} = (\lambda_{nm}\Psi^m - \lambda_{mn}\Psi^n), \tag{3.36}$$

where Ψ^m and Ψ^n are the stationary distributions corresponding to threat levels S_m and S_n, respectively. Unlike the 1-D case, this is a first order PDE system corresponding to x and y. From equation (3.35), we get Ψ^n in terms of Ψ^m as following

$$\Psi^n = \frac{a_m}{\lambda_{mn}}\Psi^m_x + \frac{r_m}{\lambda_{mn}}\Psi^m_y + \frac{\lambda_{nm}}{\lambda_{mn}}\Psi^m, \tag{3.37}$$

then substitute Ψ^n into equation(3.36), we obtain second order PDE of Ψ^m corresponding to x and y:

$$a_m a_n \Psi^m_{xx} + (a_m r_n + a_n r_m)\Psi^m_{xy} + r_m r_n \Psi^m_{yy} + (\lambda_{mn} a_m + \lambda_{nm} a_n)\Psi^m_x + (\lambda_{mn} r_m + \lambda_{nm} r_n)\Psi^m_y = 0 \tag{3.38}$$

Therefore, we achieve the following results,

Theorem 3.2.1. *When $a_m r_n - a_n r_m \neq 0$, the resulting equation(3.38) is Hyperbolic with stationary solutions Ψ^m and Ψ^n given by*

$$\Psi^m(x, y) = Ke^{\gamma_1 x - \gamma_2 y} \tag{3.39}$$

and

$$\Psi^n(x, y) = \left(\frac{a_m}{\lambda_{mn}}\gamma_1 - \frac{r_m}{\lambda_{mn}}\gamma_2 + \frac{\lambda_{nm}}{\lambda_{mn}}\right) Ke^{\gamma_1 x - \gamma_2 y} \tag{3.40}$$

where

$$\gamma_1 = \omega \left[\frac{\lambda_{nm} r_n}{1 - \omega(a_m r_n - a_n r_m)} + \lambda_{mn} r_m \right] \tag{3.41}$$

and

$$\gamma_2 = \omega \left[\frac{\lambda_{mn} a_n}{1 - \omega(a_m r_n - a_n r_m)} + \lambda_{nm} a_m \right] \tag{3.42}$$

and K and ω are constants depending on the boundary conditions.

Proof. To solve the equation (3.38), we use canonical form. Let $\Psi^m(x, y) = U(\zeta(x, y), \eta(x, y))$, the canonical variables ζ and η for a hyperbolic pde satisfy the equations

$$\begin{aligned} A\zeta_x + (B + \sqrt{B^2 - AC})\zeta_y = 0 \\ A\eta_x + (B - \sqrt{B^2 - AC})\eta_y = 0, \end{aligned} \tag{3.43}$$

where $A = a_m a_n$, $B = \frac{1}{2}(a_m r_n + a_n r_m)$ and $C = r_m r_n$. Then equation (3.43) reduced to

$$\begin{aligned} \zeta_x + \frac{r_n}{a_n}\zeta_y = 0 \\ \eta_x + \frac{r_m}{a_m}\eta_y = 0. \end{aligned} \tag{3.44}$$

Solving these equations by the method of characteristics, and for simplicity we take

$$\begin{aligned} \zeta = \frac{r_n}{a_n}x - y \\ \eta = \frac{r_m}{a_m}x - y \end{aligned} \tag{3.45}$$

Thus equation (3.38) reduces to

$$(a_m r_n - a_n r_m)U_{\zeta\eta} - \lambda_{mn} a_m U_\zeta + \lambda_{nm} a_n U_\eta = 0. \tag{3.46}$$

Then we use separation of variables to solve equation (3.46), let $U(\zeta, \eta) = X(\zeta)T(\eta)$, equation (3.46) becomes

$$(a_m r_n - a_n r_m)X'T' - \lambda_{mn} a_m X'T + \lambda_{nm} a_n XT' = 0. \tag{3.47}$$

Then there is a constant ω such that

$$\frac{X'}{(a_m r_n - a_n r_m)X' + \lambda_{nm} X} = \frac{T'}{\lambda_{mn} a_m T} = \omega. \tag{3.48}$$

Solve equation (3.48) for $X(\zeta)$ and $T(\eta)$ respectively

$$X(\zeta) = c_1 e^{\frac{\omega\lambda_{nm}a_n}{1-\omega(a_m r_n - a_n r_m)}\zeta} \tag{3.49}$$

and

$$T(\eta) = c_2 e^{\omega\lambda_{mn}a_m\eta}. \tag{3.50}$$

where c_1 and c_2 are constants. Thus

$$U(\zeta, \eta) = X(\zeta)T(\eta) = Ke^{\frac{\omega\lambda_{nm}a_n}{1-\omega(a_m r_n - a_n r_m)}\zeta + \omega\lambda_{mn}a_m\eta} \tag{3.51}$$

where K is a constant. Then we substitute euqation (3.45) into equation (3.51), we get the general solution

$$\Psi^m(x,y) = Ke^{\gamma_1 x - \gamma_2 y}, \tag{3.52}$$

and

$$\Psi^n(x,y) = \left(\frac{a_m}{\lambda_{mn}}\gamma_1 - \frac{r_m}{\lambda_{mn}}\gamma_2 + \frac{\lambda_{nm}}{\lambda_{mn}}\right) Ke^{\gamma_1 x - \gamma_2 y} \tag{3.53}$$

where

$$\gamma_1 = \omega\left[\frac{\lambda_{nm}r_n}{1-\omega(a_m r_n - a_n r_m)} + \lambda_{mn}r_m\right] \tag{3.54}$$

and

$$\gamma_2 = \omega\left[\frac{\lambda_{mn}a_n}{1-\omega(a_m r_n - a_n r_m)} + \lambda_{nm}a_m\right] \tag{3.55}$$

and C and ω are constants depending on the boundary conditions. □

Theorem 3.2.2. *When $a_m r_n - a_n r_m = 0$, the resulting equations(3.38) are Parabolic with stationary solutions Ψ^m and Ψ^n given by*

$$\Psi^m(x,y) = f\left(\frac{r_m}{a_m}x - y\right)e^{-\left(\frac{\lambda_{mn}}{a_n}+\frac{\lambda_{nm}}{a_m}\right)x} + g\left(\frac{r_m}{a_m}x - y\right) \tag{3.56}$$

and

$$\Psi^n(x,y) = -\frac{a_m}{a_n} f\left(\frac{r_m}{a_m}x - y\right) e^{-\left(\frac{\lambda_{mn}}{a_n}+\frac{\lambda_{nm}}{a_m}\right)x} + \frac{\lambda_{nm}}{\lambda_{mn}} g\left(\frac{r_m}{a_m}x - y\right) \tag{3.57}$$

where f and g are smooth function depending on boundary conditions.

Proof. If $a_m r_n - a_n r_m = 0$, then equation (3.38) reduces to

$$a_m a_n \Psi^m xx + 2a_m r_n \Psi^m xy + r_m r_n \Psi^m_{yy} + (\lambda_{mn} a_m + \lambda_{nm} a_n)\Psi^m_x + (\lambda_{mn} r_m + \lambda_{nm} r_n)\Psi^m_y = 0. \tag{3.58}$$

Similar to the proof of Theorem (3.2.1), we use canonical form. Let $u(x,y) = U(\zeta(x,y), \eta(x,y))$, the canonical variables ζ and η for a parabolic pde satisfy the equation

$$A\zeta_x + B\zeta_y = 0 \tag{3.59}$$

where $A = a_m a_n$, $B = \frac{1}{2}(a_m r_n + a_n r_m)$ Then equation (3.59) reduced to

$$\zeta_x + \frac{r_m}{a_m}\zeta_y = 0 \tag{3.60}$$

Solving equation (3.60) by the method of characteristics, and for simplicity we take

$$\zeta = \frac{r_m}{a_m}x - y \tag{3.61}$$

$$\eta = x. \tag{3.62}$$

Thus, equation (3.58) reduces to

$$a_m a_n U_{\eta\eta} + (\lambda_{mn} a_m + \lambda_{nm} a_n) U_\eta = 0. \tag{3.63}$$

Equation (3.63) is just an second order ode corresponding to η, solve it, we get

$$U(\zeta, \eta) = f(\zeta) e^{-\left(\frac{\lambda_{mn}}{a_n} + \frac{\lambda_{nm}}{a_m}\right)\eta} + g(\zeta), \tag{3.64}$$

where f and g are smooth function depending on boundary conditions. Then substitute equation (3.62) into equation (3.64), we have the general solutions

$$\Psi^m(x, y) = f\left(\frac{r_m}{a_m}x - y\right) e^{-\left(\frac{\lambda_{mn}}{a_n} + \frac{\lambda_{nm}}{a_m}\right)x} + g\left(\frac{r_m}{a_m}x - y\right) \tag{3.65}$$

and

$$\Psi^n(x, y) = -\frac{a_m}{a_n} f\left(\frac{r_m}{a_m}x - y\right) e^{-\left(\frac{\lambda_{mn}}{a_n} + \frac{\lambda_{nm}}{a_m}\right)x} + \frac{\lambda_{nm}}{\lambda_{mn}} g\left(\frac{r_m}{a_m}x - y\right). \tag{3.66}$$

□

When the system failure rates is not changed by malevolent actions, $\lambda_{mn} = \lambda_{nm} = \lambda$ yielding the following results

Corollary 3.2.1. *Let $\lambda_{mn} = \lambda_{nm} = \lambda$ in Theorem 3.2.1, then we get the Hyperbolic equations with stationary solutions Ψ^m and Ψ^n given by*

$$\Psi^m(x, y) = Ce^{\gamma_1 x - \gamma_2 y} \tag{3.67}$$

and

$$\Psi^n(x, y) = \left(\frac{a_m}{\lambda_{mn}} \gamma_1 - \frac{r_m}{\lambda_{mn}} \gamma_2 + 1 \right) Ke^{\gamma_1 x - \gamma_2 y} \tag{3.68}$$

where

$$\gamma_1 = \omega\lambda \left[\frac{r_n}{1 - \omega(a_m r_n - a_n r_m)} + r_m \right], \tag{3.69}$$

$$\gamma_2 = \omega\lambda \left[\frac{a_n}{1 - \omega(a_m r_n - a_n r_m)} + a_m \right], \tag{3.70}$$

and C and ω are constants depending on the boundary conditions.

Proof. Just substitute $\lambda_{mn} = \lambda_{nm} = \lambda$ into the solutions in Theorem 3.2.1 □

Corollary 3.2.2. *Let $\lambda_{mn} = \lambda_{nm} = \lambda$ in Theorem 3.2.2, then we get the Parabolic equations with stationary solutions Ψ^m and Ψ^n given by*

$$\Psi^m(x,y) = f\left(\frac{r_m}{a_m}x - y\right) e^{-\lambda\left(\frac{1}{a_n}+\frac{1}{a_m}\right)x} + g\left(\frac{r_m}{a_m}x - y\right) \tag{3.71}$$

and

$$\Psi^n(x,y) = -\frac{a_m}{a_n} f\left(\frac{r_m}{a_m}x - y\right) e^{-\left(\frac{\lambda_{mn}}{a_n}+\frac{\lambda_{nm}}{a_m}\right)x} + g\left(\frac{r_m}{a_m}x - y\right) \tag{3.72}$$

where f and g are smooth function depending on boundary conditions.

Proof. Similiar as Corollary 3.2.1 □

Chapter 4

Numerical Experiments and Results

In this chapter, we want to verify the results in Chapter 2 and Chapter 3 by numerical computation. Depending on the numerical results, on the one hand, we can verify the computation and theorems, on the other hand, we can have a better understanding of how to use these theorems and corollaries. Next, we present an example, similar to the work of Parthasarathy and Vijayashree [37], to illustrate our proposed technique.

4.1 Eigenvalue Spectrum for 1-D SFQs

In this section, a process is devised that incorporates the transient analysis of Chapter 2 for determining definitive solutions W^m and W^n. This method consists of the following three components:

1) *Compute Eigenvalues* This module calculates the eigenvalues while considering both Markovian and Poisson transitions. Here, Theorem 2.1.1 is employed to identify the unstable eigenvalues as well as their corresponding Fourier modes.

2) *Compute Coefficients* Once the appropriate eigenvalues have been determined, the coefficients, B_k and C_k, are determined via (17) and (18). To ensure stable solutions, B_k is set to zero at each unstable corresponding mode.

3) *Compute Series Solution* Next, the results of Steps 1 and 2 are compiled to produce closed-form solutions.

Table 4.1: Eigenvalue Spectrum Per Fourier Mode.

Fourier Mode k	Eigenvalue $c_1(k)$	Eigenvalue $c_2(k)$
0	0	-7.250
1	-0.017-j2.50	-7.233-j2.50
2	-0.105-j5.00	-7.145-j5.00
3	-0.268-j7.50	-6.982-j7.50
4	-0.518-j10.00	-6.732-j10.00

Table 4.1 ... continued

A	B	C
5	-0.878-j12.50	-6.372-j12.50
6	-1.398-j15.00	-5.852-j15.00
7	-2.168-j17.50	-5.082-j17.50
8	-1.618-j20.00	-5.632-j20.00
9	-0.740-j22.50	-6.510-j22.50
10	0.005-j25.00	-7.255-j25.00
11	0.681-j27.50	-7.931-j27.50
12	1.316-j30.00	-8.566-j30.00

Table 4.2: Eigenvalue Spectrum Per Fourier Mode.

Fourier Mode k	Eigenvalue $c_1(k)$	Eigenvalue $c_2(k)$
0	0	-7.250
-1	-0.017+j2.50	-7.233+j2.50
-2	-0.105+j5.00	-7.145+j5.00
-3	-0.268+j7.50	-6.982+j7.50
-4	-0.518+j10.00	-6.732+j10.00
-5	-0.878+j12.50	-6.372+j12.50
-6	-1.398+j15.00	-5.852+j15.00
-7	-2.168+j17.50	-5.082+j17.50

Table 4.2 ... continued

A	B	C
-8	-1.618+j20.00	-5.632+j20.00
-9	-0.740+j22.50	-6.510+j22.50
-10	0.005+j25.00	-7.255+j25.00
-11	0.681+j27.50	-7.931+j27.50
-12	1.316+j30.00	-8.566+j30.00

Tables 4.1 and 4.2 present the eigenvalue spectrum for $\lambda_{mn} = 3.75$, $\lambda_{nm} = 3.5$, $a_m = 2$ and $a_n = 3$. It is important to note the occurrence of unstable eigenvalues c_1 when $k \in [10, 12]$. This illustrates the importance of Theorem 2.1.1 because the instability of W^m and W^n depends on the behavior of $c_{1,2}(k)$ which are based on the attack and system failure rates. Although instability can be determined with $c_r(k) > 0$, Theorem 2.1.1 shows that these unstable modes are based on the combination of a_m, a_n, λ_{mn} and λ_{nm}. This result is more robust because it connects the instability behavior to the combination of the system and attack rates.

When $\lambda_{mn} = \lambda_{nm} = \lambda$ all of the eigenvalues, c_1 and c_2 are stable. This is consistent with Theorem 2.1.2 where Tables 4.3 and 4.4 show the eigenvalue spectrum for the case where $a_m = 2$, $a_n = 3$,and $\lambda_{mn} = \lambda_{nm} = 3.5$. For each mode, the real part of each eigenvalue is either less than or equal to zero. This behavior is consistent regardless of the unchanging system failure rate λ and the cyber attack rates. It is

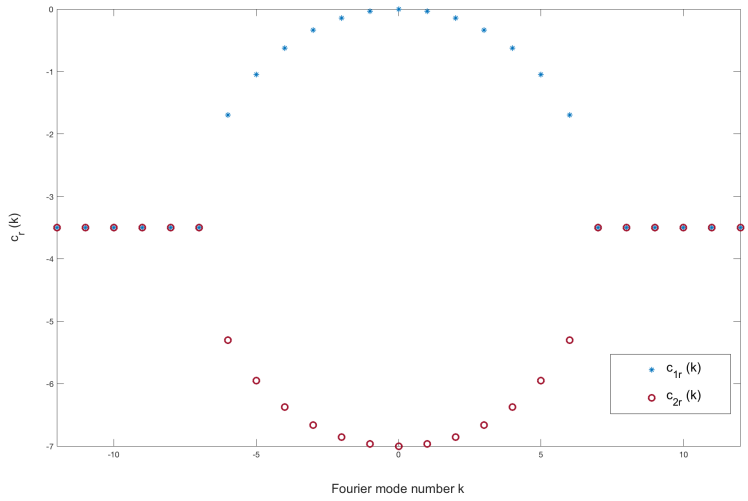

Figure 4.1: Growth rate spectrum for $\lambda = 3.5$, $a_m = 2$ and $a_n = 3$ for $k \in [-12, 12]$

also important to notice the behavior of the decay rate given by $Re(c_{1,2}(k))$ shown in Figure 4.1. As k approaches 7, the decay rate converges to 3.5, which supports Corollary 2.1.1.

Table 4.3: Eigenvalue Spectrum Per Fourier Mode.

Fourier Mode k	Eigenvalue $c_1(k)$	Eigenvalue $c_2(k)$
0	0	-7
1	-0.036+j2.50	-6.964+j2.50
2	-0.146+j5.00	-6.854+j5.00
3	-0.338+j7.50	-6.662+j7.50
4	-0.628+j10.00	-6.372+j10.00
5	-1.051+j12.50	-5.950+j12.50
6	-1.697+j15.00	-5.303+j15.00

Table 4.3 ... continued

A	B	C
7	-3.500+j17.50	-3.500+j17.50
8	-3.500+j21.94	-3.500+j18.06
9	-3.500+j25.33	-3.500+j19.67
10	-3.500+j28.57	-3.500+j21.43
11	-3.500+j31.74	-3.500+j23.28
12	-3.500+j34.87	-3.500+j25.13

Table 4.4: Eigenvalue Spectrum Per Fourier Mode.

Fourier Mode k	Eigenvalue $c_1(k)$	Eigenvalue $c_2(k)$
0	0	-7
-1	-0.036-j2.50	-6.964-j2.50
-2	-0.146-j5.00	-6.854-j5.00
-3	-0.338-j7.50	-6.662-j7.50
-4	-0.628-j10.00	-6.372-j10.00
-5	-1.051-j12.50	-5.950-j12.50
-6	-1.697-j15.00	-5.303-j15.00
-7	-3.500-j17.50	-3.500-j17.50
-8	-3.500-j18.06	-3.500-j21.94
-9	-3.500-j19.67	-3.500-j25.33

Table 4.4 ... continued

A	B	C
-10	-3.500-j21.43	-3.500-j28.57
-11	-3.500-j23.28	-3.500-j31.74
-12	-3.500-j25.13	-3.500-j34.87

4.2 Eigenvalue Spectrum for 2-D SFQs

Similarly, for $\lambda_{mn} = 3.75$, $\lambda_{nm} = 3.5$, $a_m = 2$, $a_n = 3$, $r_m = 2$ and $r_n = 1$, Tables 4.5 through 4.8 present the real and imaginary part of eigenvalue spectrum of c_1, Tables 4.9 through 4.12 present the real and imaginary part of eigenvalue spectrum of c_2. It is important to note the occurrence of unstable eigenvalues c_1, when the couple k, l takes different values. This illustrates the importance of Theorem 3.1.1 because the instability of W^m and W^n depends on the behavior of $c_{1,2}(k, l)$ which are based on the attack, infected application, and system failure rates. Although instability can be determined with $c_r(k, l) > 0$, Theorem 3.1.1 shows that these unstable modes are based on the combination of a_m, a_n, r_m, r_n, λ_{mn} and λ_{nm}. This result is more robust because it connects the instability behavior to the combination of the system, attack and infected application rates.

For $\lambda_{mn} = \lambda_{nm} = \lambda = 3.5$, $a_m = 2$, $a_n = 3$, $r_m = 2$ and $r_n = 1$. Table 4.13 through 4.16 present the real and imaginary part of eigenvalue spectrum of c_1, Table

Table 4.5: Real Part of Eigenvalue Spectrum of c_1 Per Fourier Mode for $k, l \in [0, 12]$, when $\lambda_{mn} \neq \lambda_{nm}$.

k \ l	0	1	2	3	4	5	6	7	8	9	10	11	12
0	3.378	3.311	3.107	2.753	2.221	1.458	0.343	-1.427	-0.249	1.563	3.049	4.381	5.623
1	3.311	3.244	3.037	2.679	2.140	1.365	0.223	-1.591	-0.127	1.649	3.117	4.438	5.673
2	3.106	3.037	2.824	2.452	1.892	1.076	-0.155	-1.815	0.233	1.903	3.320	4.609	5.821
3	2.750	2.677	2.451	2.055	1.451	0.552	-0.881	-1.183	0.781	2.306	3.646	4.886	6.064
4	2.216	2.135	1.887	1.448	0.762	-0.313	-2.027	-0.163	1.458	2.829	4.080	5.260	6.395
5	1.447	1.353	1.064	0.539	-0.327	-1.881	-0.757	0.870	2.220	3.447	4.605	5.719	6.804
6	0.308	0.186	-0.201	-0.961	-2.461	-0.785	0.650	1.888	3.037	4.136	5.205	6.252	7.285
7	-1.771	-2.069	-2.972	-1.364	-0.211	0.855	1.883	2.892	3.890	4.880	5.866	6.847	7.826
8	-0.351	-0.217	0170	0.743	1.437	2.209	3.031	3.888	4.768	5.666	6.576	7.495	8.421
9	1.528	1.616	1.876	2.285	2.815	3.437	4.131	4.877	5.664	6.483	7.325	8.186	9.062
10	3.029	3.098	3.303	3.632	4.069	4.597	5.199	5.862	6.574	7.324	8.106	8.913	9.742
11	4.367	4.424	4.596	4.875	5.251	5.712	6.247	6.844	7.492	8.184	8.913	9.672	0.456
12	5.612	5.662	5.811	6.055	6.387	6.798	7.280	7.823	8.419	9.060	9.741	10.455	11.198

Table 4.6: Imaginary Part of Eigenvalue Spectrum of c_1 Per Fourier Mode for $k, l \in [0, 12]$, when $\lambda_{mn} \neq \lambda_{nm}$.

k \ l	0	1	2	3	4	5	6	7	8	9	10	11	12
0	0	-1.500	-3.000	-4.500	-6.000	-7.500	-9.000	-10.500	-12.000	-13.500	-15.000	-16.500	-18.000
1	-2.500	-4.000	-5.500	-7.000	-8.500	-10.000	-11.500	-13.000	-14.500	-16.000	-17.500	-19.000	-20.500
2	-5.000	-6.500	-8.000	-9.500	-11.000	-12.500	-14.000	-15.500	-17.000	-18.500	-20.000	-21.500	-23.000
3	-7.500	-9.000	-10.500	-12.000	-13.500	-15.000	-16.500	-18.000	-19.500	-21.000	-22.500	-24.000	-25.500
4	-10.000	-11.500	-13.000	-14.500	-16.000	-17.500	-19.000	-20.500	-22.000	-23.500	-25.000	-26.500	-28.000
5	-12.500	-14.000	-15.500	-17.000	-18.500	-20.000	-21.500	-23.000	-24.500	-26.000	-27.500	-29.000	-30.500
6	-15.000	-16.500	-18.000	-19.500	-21.000	-22.500	-24.000	-25.500	-27.000	-28.500	-30.000	-31.500	-33.000
7	-17.500	-19.000	-20.500	-22.000	-23.500	-25.000	-26.500	-28.000	-29.500	-31.000	-32.500	-34.000	-35.500
8	-20.000	-21.500	-23.000	-24.500	-26.000	-27.500	-29.000	-30.500	-32.000	-33.500	-35.000	-36.500	-38.000
9	-22.500	-24.000	-25.500	-27.000	-28.500	-30.000	-31.500	-33.000	-34.500	-36.000	-37.500	-39.000	-40.500
10	-25.000	-26.500	-28.000	-29.500	-31.000	-32.500	-34.000	-35.500	-37.000	-38.500	-40.000	-41.500	-43.000
11	-27.500	-29.000	-30.500	-32.000	-33.500	-35.000	-36.500	-38.000	-39.500	-41.000	-42.500	-44.000	-45.500
12	-30.000	-31.500	-33.000	-34.500	-36.000	-37.500	-39.000	-40.500	-42.000	-43.500	-45.000	-46.500	-48.000

4.17 through 4.20 present the real and imaginary part of eigenvalue spectrum of c_2.

This is consistent with Theorem 3.1.2

Table 4.7: Real Part of Eigenvalue Spectrum of c_1 Per Fourier Mode for $k, l \in [-12, 0]$, when $\lambda_{mn} \neq \lambda_{nm}$.

k \ l	0	-1	-2	-3	-4	-5	-6	-7	-8	-9	-10	-11	-12
0	3.378	3.311	3.107	2.753	2.221	1.458	0.343	-1.427	-0.249	1.563	3.049	4.381	5.623
-1	3.311	3.244	3.037	2.679	2.140	1.365	0.223	-1.591	-0.127	1.649	3.117	4.438	5.673
-2	3.106	3.037	2.824	2.452	1.892	1.076	-0.155	-1.815	0.233	1.903	3.320	4.609	5.821
-3	2.750	2.677	2.451	2.055	1.451	0.552	-0.881	-1.183	0.781	2.306	3.646	4.886	6.064
-4	2.216	2.135	1.887	1.448	0.762	-0.313	-2.027	-0.163	1.458	2.829	4.080	5.260	6.395
-5	1.447	1.353	1.064	0.539	-0.327	-1.881	-0.757	0.870	2.220	3.447	4.605	5.719	6.804
-6	0.308	0.186	-0.201	-0.961	-2.461	-0.785	0.650	1.888	3.037	4.136	5.205	6.252	7.285
-7	-1.771	-2.069	-2.972	-1.364	-0.211	0.855	1.883	2.892	3.890	4.880	5.866	6.847	7.826
-8	-0.351	-0.217	0170	0.743	1.437	2.209	3.031	3.888	4.768	5.666	6.576	7.495	8.421
-9	1.528	1.616	1.876	2.285	2.815	3.437	4.131	4.877	5.664	6.483	7.325	8.186	9.062
-10	3.029	3.098	3.303	3.632	4.069	4.597	5.199	5.862	6.574	7.324	8.106	8.913	9.742
-11	4.367	4.424	4.596	4.875	5.251	5.712	6.247	6.844	7.492	8.184	8.913	9.672	0.456
-12	5.612	5.662	5.811	6.055	6.387	6.798	7.280	7.823	8.419	9.060	9.741	10.455	11.198

Table 4.8: Imaginary Part of Eigenvalue Spectrum of c_1 Per Fourier Mode for $k, l \in [-12, 0]$, when $\lambda_{mn} \neq \lambda_{nm}$.

k \ l	0	-1	-2	-3	-4	-5	-6	-7	-8	-9	-10	-11	-12
0	0	1.500	3.000	4.500	6.000	7.500	9.000	10.500	12.000	13.500	15.000	16.500	18.000
-1	2.500	4.000	5.500	7.000	8.500	10.000	11.500	13.000	14.500	16.000	17.500	19.000	20.500
-2	5.000	6.500	8.000	9.500	11.000	12.500	14.000	15.500	17.000	18.500	20.000	21.500	23.000
-3	7.500	9.000	10.500	12.000	13.500	15.000	16.500	18.000	19.500	21.000	22.500	24.000	25.500
-4	10.000	11.500	13.000	14.500	16.000	17.500	19.000	20.500	22.000	23.500	25.000	26.500	28.000
-5	12.500	14.000	15.500	17.000	18.500	20.000	21.500	23.000	24.500	26.000	27.500	29.000	30.500
-6	15.000	16.500	18.000	19.500	21.000	22.500	24.000	25.500	27.000	28.500	30.000	31.500	33.000
-7	17.500	19.000	20.500	22.000	23.500	25.000	26.500	28.000	29.500	31.000	32.500	34.000	35.500
-8	20.000	21.500	23.000	24.500	26.000	27.500	29.000	30.500	32.000	33.500	35.000	36.500	38.000
-9	22.500	24.000	25.500	27.000	28.500	30.000	31.500	33.000	34.500	36.000	37.500	39.000	40.500
-10	25.000	26.500	28.000	29.500	31.000	32.500	34.000	35.500	37.000	38.500	40.000	41.500	43.000
-11	27.500	29.000	30.500	32.000	33.500	35.000	36.500	38.000	39.500	41.000	42.500	44.000	45.500
-12	30.000	31.500	33.000	34.500	36.000	37.500	39.000	40.500	42.000	43.500	45.000	46.500	48.000

Table 4.9: Real Part of Eigenvalue Spectrum of c_2 Per Fourier Mode for $k, l \in [0, 12]$, when $\lambda_{mn} \neq \lambda_{nm}$.

k \ l	0	1	2	3	4	5	6	7	8	9	10	11	12
0	-10.628	-10.561	-10.357	-10.003	-9.471	-8.708	-7.593	-5.823	-7.001	-8.813	-10.299	-11.631	-12.873
1	-10.561	-10.495	-10.287	-9.929	-9.390	-8.615	-7.473	-5.659	-7.123	-8.899	-10.367	-11.688	-12.923
2	-10.356	-10.287	-10.074	-9.702	-9.142	-8.326	-7.095	-5.435	-7.483	-9.153	-10.570	-11.859	-13.071
3	-10.000	-9.927	-9.701	-9.305	-8.701	-7.802	-6.369	-6.067	-8.031	-9.556	-10.896	-12.136	-13.314
4	-9.466	-9.385	-9.137	-8.698	-8.012	-6.938	-5.223	-7.087	-8.708	-10.079	-11.330	-12.510	-13.645
5	-8.697	-8.603	-8.314	-7.789	-6.923	-5.369	-6.493	-8.120	-9.470	-10.697	-11.855	-12.969	-14.054
6	-7.558	-7.436	-7.049	-6.289	-4.790	-6.465	-7.900	-9.138	-10.287	-11.386	-12.455	-13.502	-14.535
7	-5.479	-5.181	-4.278	-5.886	-7.040	-8.105	-9.133	-10.142	-11.140	-12.130	-13.116	-14.097	-15.076
8	-6.899	-7.033	-7.420	-7.993	-8.687	-9.459	-10.281	-11.138	-12.018	-12.916	-13.826	-14.745	-15.671
9	-8.778	-8.866	-9.126	-9.535	-10.065	-10.687	-11.381	-12.127	-12.914	-13.733	-14.575	-15.436	-16.312
10	-10.279	-10.348	-10.553	-10.882	-11.319	-11.847	-12.449	-13.112	-13.824	-14.573	-15.356	16.163	-16.992
11	-11.617	-11.674	-11.846	-12.125	-12.501	-12.962	-13.497	-14.094	-14.742	-15.434	-16.163	-16.922	-17.706
12	-12.862	-12.912	-13.061	-13.305	-13.637	-14.048	-14.530	-15.073	-15.669	-16.310	-16.991	-17.705	-18.448

Table 4.10: Imaginary Part of Eigenvalue Spectrum of c_2 Per Fourier Mode for $k, l \in [0, 12]$, when $\lambda_{mn} \neq \lambda_{nm}$.

k \ l	0	1	2	3	4	5	6	7	8	9	10	11	12
0	0	-1.500	-3.000	-4.500	-6.000	-7.500	-9.000	-10.500	-12.000	-13.500	-15.000	-16.500	-18.000
1	-2.500	-4.000	-5.500	-7.000	-8.500	-10.000	-11.500	-13.000	-14.500	-16.000	-17.500	-19.000	-20.500
2	-5.000	-6.500	-8.000	-9.500	-11.000	-12.500	-14.000	-15.500	-17.000	-18.500	-20.000	-21.500	-23.000
3	-7.500	-9.000	-10.500	-12.000	-13.500	-15.000	-16.500	-18.000	-19.500	-21.000	-22.500	-24.000	-25.500
4	-10.000	-11.500	-13.000	-14.500	-16.000	-17.500	-19.000	-20.500	-22.000	-23.500	-25.000	-26.500	-28.000
5	-12.500	-14.000	-15.500	-17.000	-18.500	-20.000	-21.500	-23.000	-24.500	-26.000	-27.500	-29.000	-30.500
6	-15.000	-16.500	-18.000	-19.500	-21.000	-22.500	-24.000	-25.500	-27.000	-28.500	-30.000	-31.500	-33.000
7	-17.500	-19.000	-20.500	-22.000	-23.500	-25.000	-26.500	-28.000	-29.500	-31.000	-32.500	-34.000	-35.500
8	-20.000	-21.500	-23.000	-24.500	-26.000	-27.500	-29.000	-30.500	-32.000	-33.500	-35.000	-36.500	-38.000
9	-22.500	-24.000	-25.500	-27.000	-28.500	-30.000	-31.500	-33.000	-34.500	-36.000	-37.500	-39.000	-40.500
10	-25.000	-26.500	-28.000	-29.500	-31.000	-32.500	-34.000	-35.500	-37.000	-38.500	-40.000	-41.500	-43.000
11	-27.500	-29.000	-30.500	-32.000	-33.500	-35.000	-36.500	-38.000	-39.500	-41.000	-42.500	-44.000	-45.500
12	-30.000	-31.500	-33.000	-34.500	-36.000	-37.500	-39.000	-40.500	-42.000	-43.500	-45.000	-46.500	-48.000

Table 4.11: Real Part of Eigenvalue Spectrum of c_2 Per Fourier Mode for $k, l \in [-12, 0]$, when $\lambda_{mn} \neq \lambda_{nm}$.

k \ l	0	-1	-2	-3	-4	-5	-6	-7	-8	-9	-10	-11	-12
0	-10.628	-10.561	-10.357	-10.003	-9.471	-8.708	-7.593	-5.823	-7.001	-8.813	-10.299	-11.631	-12.873
-1	-10.561	-10.495	-10.287	-9.929	-9.390	-8.615	-7.473	-5.659	-7.123	-8.899	-10.367	-11.688	-12.923
-2	-10.356	-10.287	-10.074	-9.702	-9.142	-8.326	-7.095	-5.435	-7.483	-9.153	-10.570	-11.859	-13.071
-3	-10.000	-9.927	-9.701	-9.305	-8.701	-7.802	-6.369	-6.067	-8.031	-9.556	-10.896	-12.136	-13.314
-4	-9.466	-9.385	-9.137	-8.698	-8.012	-6.938	-5.223	-7.087	-8.708	-10.079	-11.330	-12.510	-13.645
-5	-8.697	-8.603	-8.314	-7.789	-6.923	-5.369	-6.493	-8.120	-9.470	-10.697	-11.855	-12.969	-14.054
-6	-7.558	-7.436	-7.049	-6.289	-4.790	-6.465	-7.900	-9.138	-10.287	-11.386	-12.455	-13.502	-14.535
-7	-5.479	-5.181	-4.278	-5.886	-7.040	-8.105	-9.133	-10.142	-11.140	-12.130	-13.116	-14.097	-15.076
-8	-6.899	-7.033	-7.420	-7.993	-8.687	-9.459	-10.281	-11.138	-12.018	-12.916	-13.826	-14.745	-15.671
-9	-8.778	-8.866	-9.126	-9.535	-10.065	-10.687	-11.381	-12.127	-12.914	-13.733	-14.575	-15.436	-16.312
-10	-10.279	-10.348	-10.553	-10.882	-11.319	-11.847	-12.449	-13.112	-13.824	-14.573	-15.356	16.163	-16.992
-11	-11.617	-11.674	-11.846	-12.125	-12.501	-12.962	-13.497	-14.094	-14.742	-15.434	-16.163	-16.922	-17.706
-12	-12.862	-12.912	-13.061	-13.305	-13.637	-14.048	-14.530	-15.073	-15.669	-16.310	-16.991	-17.705	-18.448

Table 4.12: Imaginary Part of Eigenvalue Spectrum of c_2 Per Fourier Mode for $k, l \in [-12, 0]$, when $\lambda_{mn} \neq \lambda_{nm}$.

k \ l	0	-1	-2	-3	-4	-5	-6	-7	-8	-9	-10	-11	-12
0	0	1.500	3.000	4.500	6.000	7.500	9.000	10.500	12.000	13.500	15.000	16.500	18.000
-1	2.500	4.000	5.500	7.000	8.500	10.000	11.500	13.000	14.500	16.000	17.500	19.000	20.500
-2	5.000	6.500	8.000	9.500	11.000	12.500	14.000	15.500	17.000	18.500	20.000	21.500	23.000
-3	7.500	9.000	10.500	12.000	13.500	15.000	16.500	18.000	19.500	21.000	22.500	24.000	25.500
-4	10.000	11.500	13.000	14.500	16.000	17.500	19.000	20.500	22.000	23.500	25.000	26.500	28.000
-5	12.500	14.000	15.500	17.000	18.500	20.000	21.500	23.000	24.500	26.000	27.500	29.000	30.500
-6	15.000	16.500	18.000	19.500	21.000	22.500	24.000	25.500	27.000	28.500	30.000	31.500	33.000
-7	17.500	19.000	20.500	22.000	23.500	25.000	26.500	28.000	29.500	31.000	32.500	34.000	35.500
-8	20.000	21.500	23.000	24.500	26.000	27.500	29.000	30.500	32.000	33.500	35.000	36.500	38.000
-9	22.500	24.000	25.500	27.000	28.500	30.000	31.500	33.000	34.500	36.000	37.500	39.000	40.500
-10	25.000	26.500	28.000	29.500	31.000	32.500	34.000	35.500	37.000	38.500	40.000	41.500	43.000
-11	27.500	29.000	30.500	32.000	33.500	35.000	36.500	38.000	39.500	41.000	42.500	44.000	45.500
-12	30.000	31.500	33.000	34.500	36.000	37.500	39.000	40.500	42.000	43.500	45.000	46.500	48.000

Table 4.13: Real Part of Eigenvalue Spectrum of c_1 Per Fourier Mode for $k, l \in [0, 12]$, when $\lambda_{mn} = \lambda_{nm}$.

k \ l	0	1	2	3	4	5	6	7	8	9	10	11	12
0	0	-0.036	-0.072	-0.109	-0.146	-0.183	-0.221	-0.260	-0.298	-0.338	-0.378	-0.418	-0.459
1	-0.072	-0.109	-0.146	-0.183	-0.221	-0.260	-0.298	-0.338	-0.378	-0.418	-0.459	-0.500	-0.542
2	-0.146	-0.183	-0.221	-0.260	-0.298	-0.338	-0.378	-0.418	-0.459	-0.500	-0.542	-0.585	-0.628
3	-0.221	-0.260	-0.298	-0.338	-0.378	-0.418	-0.459	-0.500	-0.542	-0.585	-0.628	-0.672	-0.716
4	-0.298	-0.338	-0.378	-0.418	-0.459	-0.500	-0.542	-0.585	-0.628	-0.672	-0.716	-0.761	-0.807
5	-0.378	-0.418	-0.459	-0.500	-0.542	-0.585	-0.628	-0.672	-0.716	-0.761	-0.807	-0.854	-0.902
6	-0.459	-0.500	-0.542	-0.585	-0.628	-0.672	-0.716	-0.761	-0.807	-0.854	-0.902	-0.951	-1.000
7	-0.542	-0.585	-0.628	-0.672	-0.716	-0.761	-0.807	-0.854	-0.902	-0.951	-1.000	-1.051	-1.102
8	-0.628	-0.672	-0.716	-0.761	-0.807	-0.854	-0.902	-0.951	-1.000	-1.051	-1.102	-1.155	-1.209
9	-0.716	-0.761	-0.807	-0.854	-0.902	-0.951	-1.000	-1.051	-1.102	-1.155	-1.209	-1.264	-1.321
10	-0.807	-0.854	-0.902	-0.951	-1.000	-1.051	-1.102	-1.155	-1.209	-1.264	-1.321	-1.379	-1.438
11	-0.902	-0.951	-1.000	-1.051	-1.102	-1.155	-1.209	-1.264	-1.321	-1.379	-1.438	-1.500	-1.564
12	-1.000	-1.051	-1.102	-1.155	-1.209	-1.264	-1.321	-1.379	-1.438	-1.500	-1.564	-1.629	-1.697

Table 4.14: Imaginary Part of Eigenvalue Spectrum of c_1 Per Fourier Mode for $k, l \in [0, 12]$, when $\lambda_{mn} = \lambda_{nm}$.

k \ l	0	1	2	3	4	5	6	7	8	9	10	11	12
0	0	1.500	3.000	4.500	6.000	7.500	9.000	10.500	12.000	13.500	15.000	16.500	18.000
1	2.500	4.000	5.500	7.000	8.500	10.000	11.500	13.000	14.500	16.000	17.500	19.000	20.500
2	5.000	6.500	8.000	9.500	11.000	12.500	14.000	15.500	17.000	18.500	20.000	21.500	23.000
3	7.500	9.000	10.500	12.000	13.500	15.000	16.500	18.000	19.500	21.000	22.500	24.000	25.500
4	10.000	11.500	13.000	14.500	16.000	17.500	19.000	20.500	22.000	23.500	25.000	26.500	28.000
5	12.500	14.000	15.500	17.000	18.500	20.000	21.500	23.000	24.500	26.000	27.500	29.000	30.500
6	15.000	16.500	18.000	19.500	21.000	22.500	24.000	25.500	27.000	28.500	30.000	31.500	33.000
7	17.500	19.000	20.500	22.000	23.500	25.000	26.500	28.000	29.500	31.000	32.500	34.000	35.500
8	20.000	21.500	23.000	24.500	26.000	27.500	29.000	30.500	32.000	33.500	35.000	36.500	38.000
9	22.500	24.000	25.500	27.000	28.500	30.000	31.500	33.000	34.500	36.000	37.500	39.000	40.500
10	25.000	26.500	28.000	29.500	31.000	32.500	34.000	35.500	37.000	38.500	40.000	41.500	43.000
11	27.500	29.000	30.500	32.000	33.500	35.000	36.500	38.000	39.500	41.000	42.500	44.000	45.500
12	30.000	31.500	33.000	34.500	36.000	37.500	39.000	40.500	42.000	43.500	45.000	46.500	48.000

Table 4.15: Real Part of Eigenvalue Spectrum of c_1 Per Fourier Mode for $k, l \in [-12, 0]$, when $\lambda_{mn} = \lambda_{nm}$.

k \ l	0	-1	-2	-3	-4	-5	-6	-7	-8	-9	-10	-11	-12
0	0	0.036	0.071	0.106	0.140	0.174	0.208	0.242	0.275	0.308	0.341	0.373	0.405
-1	0.071	0.106	0.140	0.174	0.208	0.242	0.275	0.308	0.341	0.373	0.405	0.437	0.469
-2	0.140	0.174	0.208	0.242	0.275	0.308	0.341	0.373	0.405	0.437	0.469	0.500	0.531
-3	0.208	0.242	0.275	0.308	0.341	0.373	0.405	0.437	0.469	0.500	0.531	0.562	0.593
-4	0.275	0.308	0.341	0.373	0.405	0.437	0.469	0.500	0.531	0.562	0.593	0.623	0.653
-5	0.341	0.373	0.405	0.437	0.469	0.500	0.531	0.562	0.593	0.623	0.653	0.683	0.713
-6	0.405	0.437	0.469	0.500	0.531	0.562	0.593	0.623	0.653	0.683	0.713	0.743	0.772
-7	0.469	0.500	0.531	0.562	0.593	0.623	0.653	0.683	0.713	0.743	0.772	0.801	0.830
-8	0.531	0.562	0.593	0.623	0.653	0.683	0.713	0.743	0.772	0.801	0.830	0.859	0.888
-9	0.593	0.623	0.653	0.683	0.713	0.743	0.772	0.801	0.830	0.859	0.888	0.916	0.944
-10	0.653	0.683	0.713	0.743	0.772	0.801	0.830	0.859	0.888	0.916	0.944	0.972	1.000
-11	0.713	0.743	0.772	0.801	0.830	0.859	0.888	0.916	0.944	0.972	1.000	1.028	1.055
-12	0.772	0.801	0.830	0.859	0.888	0.916	0.944	0.972	1.000	1.028	1.0552	1.083	1.100

Table 4.16: Imaginary Part of Eigenvalue Spectrum of c_1 Per Fourier Mode for $k, l \in [-12, 0]$, when $\lambda_{mn} = \lambda_{nm}$.

k \ l	0	-1	-2	-3	-4	-5	-6	-7	-8	-9	-10	-11	-12
0	0	-1.500	-3.000	-4.500	-6.000	-7.500	-9.000	-10.500	-12.000	-13.500	-15.000	-16.500	-18.000
-1	-2.500	-4.000	-5.500	-7.000	-8.500	-10.000	-11.500	-13.000	-14.500	-16.000	-17.500	-19.000	-20.500
-2	-5.000	-6.500	-8.000	-9.500	-11.000	-12.500	-14.000	-15.500	-17.000	-18.500	-20.000	-21.500	-23.000
-3	-7.500	-9.000	-10.500	-12.000	-13.500	-15.000	-16.500	-18.000	-19.500	-21.000	-22.500	-24.000	-25.500
-4	-10.000	-11.500	-13.000	-14.500	-16.000	-17.500	-19.000	-20.500	-22.000	-23.500	-25.000	-26.500	-28.000
-5	-12.500	-14.000	-15.500	-17.000	-18.500	-20.000	-21.500	-23.000	-24.500	-26.000	-27.500	-29.000	-30.500
-6	-15.000	-16.500	-18.000	-19.500	-21.000	-22.500	-24.000	-25.500	-27.000	-28.500	-30.000	-31.500	-33.000
-7	-17.500	-19.000	-20.500	-22.000	-23.500	-25.000	-26.500	-28.000	-29.500	-31.000	-32.500	-34.000	-35.500
-8	-20.000	-21.500	-23.000	-24.500	-26.000	-27.500	-29.000	-30.500	-32.000	-33.500	-35.000	-36.500	-38.000
-9	-22.500	-24.000	-25.500	-27.000	-28.500	-30.000	-31.500	-33.000	-34.500	-36.000	-37.500	-39.000	-40.500
-10	-25.000	-26.500	-28.000	-29.500	-31.000	-32.500	-34.000	-35.500	-37.000	-38.500	-40.000	-41.500	-43.000
-11	-27.500	-29.000	-30.500	-32.000	-33.500	-35.000	-36.500	-38.000	-39.500	-41.000	-42.500	-44.000	-45.500
-12	-30.000	-31.500	-33.000	-34.500	-36.000	-37.500	-39.000	-40.500	-42.000	-43.500	-45.000	-46.500	-48.000

Table 4.17: Real Part of Eigenvalue Spectrum of c_2 Per Fourier Mode for $k, l \in [0, 12]$, when $\lambda_{mn} = \lambda_{nm}$.

k \ l	0	1	2	3	4	5	6	7	8	9	10	11	12
0	-7.000	-6.964	-6.928	-6.891	-6.854	-6.817	-6.779	-6.740	-6.702	-6.662	-6.623	-6.582	-6.541
1	-6.928	-6.891	-6.854	-6.817	-6.779	-6.740	-6.702	-6.662	-6.623	-6.582	-6.541	-6.500	-6.458
2	-6.854	-6.817	-6.779	-6.740	-6.702	-6.662	-6.623	-6.582	-6.541	-6.500	-6.458	-6.416	-6.372
3	-6.779	-6.740	-6.702	-6.662	-6.623	-6.582	-6.541	-6.500	-6.458	-6.416	-6.372	-6.328	-6.284
4	-6.702	-6.662	-6.623	-6.582	-6.541	-6.500	-6.458	-6.416	-6.372	-6.328	-6.284	-6.239	-6.193
5	-6.623	-6.582	-6.541	-6.500	-6.458	-6.416	-6.372	-6.328	-6.284	-6.239	-6.193	-6.146	-6.098
6	-6.541	-6.500	-6.458	-6.416	-6.372	-6.328	-6.284	-6.239	-6.193	-6.146	-6.098	-6.050	-6.000
7	-6.458	-6.416	-6.372	-6.328	-6.284	-6.239	-6.193	-6.146	-6.098	-6.050	-6.000	-5.950	-5.898
8	-6.372	-6.328	-6.284	-6.239	-6.193	-6.146	-6.098	-6.050	-6.000	-5.950	-5.898	-5.845	-5.791
9	-6.284	-6.239	-6.193	-6.146	-6.098	-6.050	-6.000	-5.950	-5.898	-5.845	-5.791	-5.736	-5.679
10	-6.193	-6.146	-6.098	-6.050	-6.000	-5.950	-5.898	-5.845	-5.791	-5.736	-5.679	-5.621	-5.562
11	-6.098	-6.050	-6.000	-5.950	-5.898	-5.845	-5.791	-5.736	-5.679	-5.621	-5.562	-5.500	-5.437
12	-6.000	-5.950	-5.898	-5.845	-5.791	-5.736	-5.679	-5.621	-5.562	-5.500	-5.437	-5.371	-5.303

Table 4.18: Imaginary Part of Eigenvalue Spectrum of c_2 Per Fourier Mode for $k, l \in [0, 12]$, when $\lambda_{mn} = \lambda_{nm}$.

k \ l	0	1	2	3	4	5	6	7	8	9	10	11	12
0	0	1.500	3.000	4.500	6.000	7.500	9.000	10.500	12.000	13.500	15.000	16.500	18.000
1	2.500	4.000	5.500	7.000	8.500	10.000	11.500	13.000	14.500	16.000	17.500	19.000	20.500
2	5.000	6.500	8.000	9.500	11.000	12.500	14.000	15.500	17.000	18.500	20.000	21.500	23.000
3	7.500	9.000	10.500	12.000	13.500	15.000	16.500	18.000	19.500	21.000	22.500	24.000	25.500
4	10.000	11.500	13.000	14.500	16.000	17.500	19.000	20.500	22.000	23.500	25.000	26.500	28.000
5	12.500	14.000	15.500	17.000	18.500	20.000	21.500	23.000	24.500	26.000	27.500	29.000	30.500
6	15.000	16.500	18.000	19.500	21.000	22.500	24.000	25.500	27.000	28.500	30.000	31.500	33.000
7	17.500	19.000	20.500	22.000	23.500	25.000	26.500	28.000	29.500	31.000	32.500	34.000	35.500
8	20.000	21.500	23.000	24.500	26.000	27.500	29.000	30.500	32.000	33.500	35.000	36.500	38.000
9	22.500	24.000	25.500	27.000	28.500	30.000	31.500	33.000	34.500	36.000	37.500	39.000	40.500
10	25.000	26.500	28.000	29.500	31.000	32.500	34.000	35.500	37.000	38.500	40.000	41.500	43.000
11	27.500	29.000	30.500	32.000	33.500	35.000	36.500	38.000	39.500	41.000	42.500	44.000	45.500
12	30.000	31.500	33.000	34.500	36.000	37.500	39.000	40.500	42.000	43.500	45.000	46.500	48.000

Table 4.19: Real Part of Eigenvalue Spectrum of c_2 Per Fourier Mode for $k, l \in [-12, 0]$, when $\lambda_{mn} = \lambda_{nm}$.

k \ l	0	-1	-2	-3	-4	-5	-6	-7	-8	-9	-10	-11	-12
0	-7.000	-7.036	-7.071	-7.106	-7.140	-7.174	-7.208	-7.242	-7.275	-7.308	-7.341	-7.373	-7.405
-1	-7.071	-7.106	-7.140	-7.174	-7.208	-7.242	-7.275	-7.308	-7.341	-7.373	-7.405	-7.437	-7.469
-2	-7.140	-7.174	-7.208	-7.242	-7.275	-7.308	-7.341	-7.373	-7.405	-7.437	-7.469	-7.500	-7.531
-3	-7.208	-7.242	-7.275	-7.308	-7.341	-7.373	-7.405	-7.437	-7.469	-7.500	-7.531	-7.562	-7.593
-4	-7.275	-7.308	-7.341	-7.373	-7.405	-7.437	-7.469	-7.500	-7.531	-7.562	-7.593	-7.623	-7.653
-5	-7.341	-7.373	-7.405	-7.437	-7.469	-7.500	-7.531	-7.562	-7.593	-7.623	-7.653	-7.683	-7.713
-6	-7.405	-7.437	-7.469	-7.500	-7.531	-7.562	-7.593	-7.623	-7.653	-7.683	-7.713	-7.743	-7.772
-7	-7.469	-7.500	-7.531	-7.562	-7.593	-7.623	-7.653	-7.683	-7.713	-7.743	-7.772	-7.801	-7.830
-8	-7.531	-7.562	-7.593	-7.623	-7.653	-7.683	-7.713	-7.743	-7.772	-7.801	-7.830	-7.859	-7.888
-9	-7.593	-7.623	-7.653	-7.683	-7.713	-7.743	-7.772	-7.801	-7.830	-7.859	-7.888	-7.916	-7.944
-10	-7.653	-7.683	-7.713	-7.743	-7.772	-7.801	-7.830	-7.859	-7.888	-7.916	-7.944	-7.972	-8.000
-11	-7.713	-7.743	-7.772	-7.801	-7.830	-7.859	-7.888	-7.916	-7.944	-7.972	-8.000	-8.028	-8.055
-12	-7.772	-7.801	-7.830	-7.859	-7.888	-7.916	-7.944	-7.972	-8.000	-8.028	-8.0552	-8.083	-8.100

Table 4.20: Imaginary Part of Eigenvalue Spectrum of c_2 Per Fourier Mode for $k, l \in [-12, 0]$, when $\lambda_{mn} = \lambda_{nm}$.

k \ l	0	-1	-2	-3	-4	-5	-6	-7	-8	-9	-10	-11	-12
0	0	-1.500	-3.000	-4.500	-6.000	-7.500	-9.000	-10.500	-12.000	-13.500	-15.000	-16.500	-18.000
-1	-2.500	-4.000	-5.500	-7.000	-8.500	-10.000	-11.500	-13.000	-14.500	-16.000	-17.500	-19.000	-20.500
-2	-5.000	-6.500	-8.000	-9.500	-11.000	-12.500	-14.000	-15.500	-17.000	-18.500	-20.000	-21.500	-23.000
-3	-7.500	-9.000	-10.500	-12.000	-13.500	-15.000	-16.500	-18.000	-19.500	-21.000	-22.500	-24.000	-25.500
-4	-10.000	-11.500	-13.000	-14.500	-16.000	-17.500	-19.000	-20.500	-22.000	-23.500	-25.000	-26.500	-28.000
-5	-12.500	-14.000	-15.500	-17.000	-18.500	-20.000	-21.500	-23.000	-24.500	-26.000	-27.500	-29.000	-30.500
-6	-15.000	-16.500	-18.000	-19.500	-21.000	-22.500	-24.000	-25.500	-27.000	-28.500	-30.000	-31.500	-33.000
-7	-17.500	-19.000	-20.500	-22.000	-23.500	-25.000	-26.500	-28.000	-29.500	-31.000	-32.500	-34.000	-35.500
-8	-20.000	-21.500	-23.000	-24.500	-26.000	-27.500	-29.000	-30.500	-32.000	-33.500	-35.000	-36.500	-38.000
-9	-22.500	-24.000	-25.500	-27.000	-28.500	-30.000	-31.500	-33.000	-34.500	-36.000	-37.500	-39.000	-40.500
-10	-25.000	-26.500	-28.000	-29.500	-31.000	-32.500	-34.000	-35.500	-37.000	-38.500	-40.000	-41.500	-43.000
-11	-27.500	-29.000	-30.500	-32.000	-33.500	-35.000	-36.500	-38.000	-39.500	-41.000	-42.500	-44.000	-45.500
-12	-30.000	-31.500	-33.000	-34.500	-36.000	-37.500	-39.000	-40.500	-42.000	-43.500	-45.000	-46.500	-48.000

4.3 Example

Next, we solve a variation of an analogous problem as in the work of Parthasarathy, [37] for the case of the 1-D stochastic fluid queue (2.4) with the initial conditions (2.5) given as

$$W^m(x,0) = f(x) = 1 \qquad \text{and} \qquad W^n(x,0) = g(x) = 0. \tag{4.1}$$

Equation (4.1) implies that the initial behavior rests solely on the malicious activity occurring at S_m. In this case, $F(k)$ and $G(k)$ become

$$F(k) = \begin{cases} 1, \text{ if } k = 0 \\ 0, \text{ otherwise,} \end{cases} \qquad \text{and} \qquad G(k) = 0 \tag{4.2}$$

Therefore, the explicit solutions become

$$W^m(x,t) = \frac{\lambda_{mn}}{\lambda_{mn} + \lambda_{nm}} + \frac{\lambda_{nm} e^{-(\lambda_{mn}+\lambda_{nm})t}}{\lambda_{mn} + \lambda_{nm}} \tag{4.3}$$

and

$$W^n(x,t) = \frac{\lambda_{nm}}{\lambda_{mn} + \lambda_{nm}} + \frac{\lambda_{nm} e^{-(\lambda_{mn}+\lambda_{nm})t}}{\lambda_{mn} + \lambda_{nm}} \tag{4.4}$$

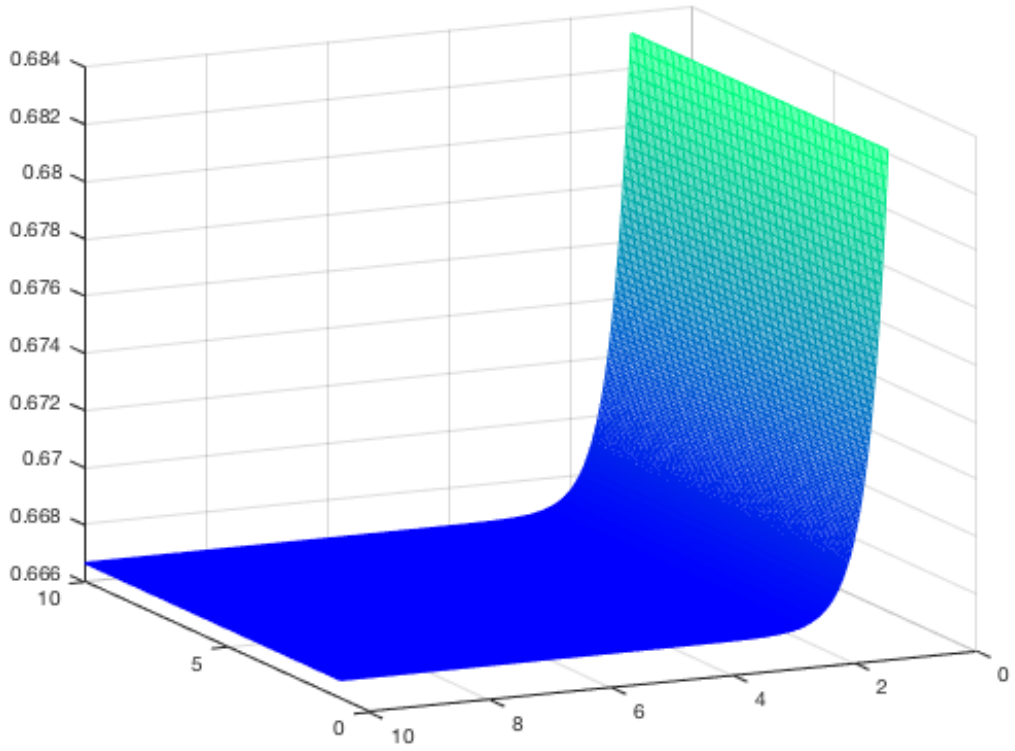

Figure 4.2: Variation of $W^m(x,t)$ for $\lambda_{mn} = 2$ and $\lambda_{nm} = 1$.

Figure 6 is a surface representation of the variation of the impact of cyber behavior within threat level S_m, where $\lambda_{mn} = 2$ and $\lambda_{nm} = 1$. This behavior gradually decreases which converge to $\frac{2}{3}$ as $t \to \infty$. From (4.4), we can determine that W^n presents opposite behavior where the probabilistic impact steadily climbs to a limit of $\frac{1}{3}$ as time increases. This behavior shows that as the cyber activity migrates between the two threat levels, the impact within each state is steadily affected. Furthermore, if the system failure rates are unaffected, then the stationary probabilities would be equally likely.

Chapter 5

Conclusion and Future Work

This thesis analyzes the impact of virulent activity within supercomputing environments for the specific case of constant dynamic switching behavior. We model these dynamics as a stochastic fluid queue fed by an ON-OFF source, where two main scenarios are considered. First, we studied the case of malicious activity affecting both the system failure rates and the threat levels, where we determined that unstable solutions depend on the combination of attack rates, system failure rates, and Fourier modes. Also we explored the case of cyber actions not affecting the system failure rates, where we find stable solutions throughout. In both scenarios, the stationary analysis for the 1-D case shows convergence to the attractive line of equilibrium governed by the system failure rates.

Similar to the 1-D case, we also determined that for 2-D case, unstable solutions depend on the combination of attack rates, infected application rates, system failure

rates, and Fourier modes in the x and y directions. Furthermore, we explored the case of cyber actions not affecting the system failure rates and infected application rates where we found stable parabolic and hyperbolic solutions throughout, which depend on the fluid rates in the x and y directions.

The numerical results in Chapter 4 verify our analyses in Chapter 2 and Chapter 3. The example also shows the ease of use of our method. Therefore, the analysis presented is more robust and comprehensive than the prior works of Faissol and Gallagher [29] and Clark [31].

The results of our work have several applications that can benefit the supercomputing community. We can apply the analysis directly to investigate the behavioral impacts of Distributed Denial of Service (DDoS), which is in the realm of intentional failures [42]. Furthermore, we can extend this methodology presented to analyzing the behavior of SFQs with multiple on-off sources. Our work can also be useful for other applications of stochastic fluid queues. The powerful element to our approach is the spectral characterization, which explicitly transforms the system of coupled partial differential equations to an eigenvalue system. From this, we can compute the instability conditions and series coefficients directly.

Future explorations of our work include generalizing this approach for understanding these effects using multiple ON-OFF sources. Although we can extend the proposed approach for this purpose, it could get computationally expensive. We also need investigations to account for situations where certain supercomputing compo-

nents are temporarily out of commission. Researching these avenues helps with the ability to attain a more comprehensive understanding of cyber phenomena within supercomputing infrastructures.

Appendix A

Codes of Phase Plane in Figure 2.3

```
[x1, x2] = meshgrid(-4:1:4, -4:1:4);
x1dot = 1/2.*x2-x1; %Note the use of .* and .^
x2dot = 2.*x1-x2;   %a=2, b=1, lambda{mn}=1, lambda{nm}=2
quiver(x1,x2,x1dot, x2dot)
xlabel('Wm')
ylabel('Wn')
title('phase plane')
xlim([-4,4])
ylim([-4,4])
grid

hold on
t=-4:1:4;
plot(t,2*t,'r')
% plot(-t,2*t,'r')
```

Appendix B

Codes of Variation of $W^m(x,t)$ in Figure 4.2

```
lambda_mn=2;
lambda_nm=1;


% Defining factors for the solution
evalFactor = lambda_mn + lambda_nm;
Factor_1m = lambda_mn/evalFactor;
Factor_1n = lambda_nm/evalFactor;

f1=Factor_1m+(Factor_1n).*exp(-evalFactor.*t);
f2=Factor_1n-(Factor_1n).*exp(-evalFactor.*t);

% t=0:0.1:10;
% plot(t,f1)
%
% xlabel('time t')
% ylabel('W^m')
% text(t,f1,'\lambda_{mn}=2, \lambda_{nm}=1')

[X,t] = meshgrid(1:.1:10,1:.01:10);
mesh(X,t,f1)
```

APPENDIX B. CODES OF VARIATION OF $W^M(X,T)$ IN FIGURE **??**

```
colormap winter
```

Appendix C

Compute Eigenvalues 1-D case

```
% ComputeEigenvalues: written by Antwan D. Clark and Ning Liu.
% This program computes the eigenvalues for 2-D the two-state stochastic fluid
% queue (SFQ) for both Markovian (lambda_mn != lambda_nm) and Poisson
% (lambda_mn = lambda_nm) cases. The eigenvalues are computed for each
% Fourier mode, which is part of the exact solutions for W^m and W^n.
%
% For the Markovian Case, this program takes into account the stability of
% the solutions via estimating the range of Fourier modes where each mode
% of the solutions W^m and W^n are stable. From this, the same program can
% be used for a spectrum of stable eigenvalues. These eigenvalues can be
% incorporated to produce approximate solutions for W^m and W^n.
%
% Input Parameters:
%  1.) lambda_mn -- System failure rate going from State m to State n.
%  2.) lambda_nm -- System failure rate going from State n to State m.
%  3.) a_m -- cyber attack rate in State m
%  4.) a_n -- cyber attafck rate in State n.
%  5.) K -- the magnitude of the maximum Fourier mode number. The span of
%  Fourier modes ranges from -K to K.
%
% Output Parameters:


% Step 1: Defining input parameters. (Right now, just test for Poisson
```

```
% Case)
lambda_mn = 3.75;
lambda_nm = 3.5;
K = 12;
a_m = 2;
a_n = 3;

%Step 2: Allocating the eigenvalue spectrum
kk = -K:K;

%Prestep: initializing vectors
c1 = zeros(1,length(kk));
c2 = zeros(1,length(kk));
phi = zeros(1, length(kk)); % This is for the Poisson case.

% Initializing for the Markovian case as well as preparing for Theorem 1.
RSquared = zeros(1, length(kk));
phi_k = zeros(1, length(kk));
varpi_k = zeros(1, length(kk));

%Allocating for recording unstable eigenvalues and modes
c1_unstable = zeros(1,length(kk));
kk_unstable = zeros(1,length(kk));
count = 1; %initializing counter for recording unstable modes.

% This is to keep track of the associate location within the vector
% corresponding to the unstable modes.
unstableIndex = zeros(1,length(kk));

% Step 2: Compute eigenvalues for each mode. If lambda_mn = lambda_nm, then
% all of the eigenvalues are stable since the real part is always
% non-positive (i.e. <= 0). Otherwise, we would need to check the
% conditions based on Theorem 1.

if lambda_mn ==lambda_nm %Poisson case.
lambda = lambda_mn;
for j = 1:length(kk)
phi(j) = sqrt(lambda^2 - kk(j)^2*((a_n - a_m)/2)^2);
c1(j) = -lambda + 1i*kk(j)*((a_m + a_n)/2) + phi(j);
c2(j) = -lambda + 1i*kk(j)*((a_m + a_n)/2) - phi(j);
end % end for loop
else %lambda_mn != lambda_nm (Markov case).
```

```
for j =1:length(kk)
% Step 2a: Computing R^2, phi_k, and varpi_k
RSquared(j) = ((lambda_mn + lambda_nm)^2 -(kk(j))^2*(a_n - a_m)^2)^2
+ 4*(kk(j))^2*(a_n - a_m)^2*(lambda_mn - lambda_nm)^2;
R(j) = sqrt(RSquared(j));
phi_k(j) = sqrt((R(j) + ((lambda_mn + lambda_nm)^2
-(kk(j))^2*(a_n - a_m)^2))/2);
varpi_k(j) = sqrt((R(j) - ((lambda_mn + lambda_nm)^2
-(kk(j))^2*(a_n - a_m)^2))/2);

%Step 2b: Compute eigenvalue spectrum
c1(j) = -((lambda_mn + lambda_nm) + 1i*kk(j)*(a_m + a_n))/2
+ (phi_k(j) + varpi_k(j))/2;
c2(j) = -((lambda_mn + lambda_nm) + 1i*kk(j)*(a_m + a_n))/2
- (phi_k(j) + varpi_k(j))/2;

%Step 3: Apply Theorem 1. The goal is to perform a check to determine
%whether the eigenvalue falls within the instability region defined in
%Theorem 1. If it does, then the eigenvalue, Fourier mode, and location
%within each vector is recorded.
dist = (real(c1(j) + ((lambda_mn + lambda_nm)/2)^2
+ (imag(c1(j)) +kk(j)*(a_m + a_n)/2)^2));
if (real(c1(j)) > 0 && dist <= RSquared(j)/4)
c1_unstable(count) = c1(j); % Recording unstable eigenvalue
kk_unstable(count) = kk(j); % Recording corresponding unstable mode.
unstableIndex(count) = j; % Recording corresponding index.
count =count+ 1;
end
end
end

% Next, gathering the growth rate data to plot corresponding to each
% Fourier mode.
```

Appendix D

Compute Eigenvalues 2-D case

```
% ComputeEigenvalues: written by Antwan D. Clark and Ning Liu.
% This program computes the eigenvalues for 3-D the two-state stochastic fluid
% queue (SFQ) for both Markovian (lambda_mn != lambda_nm) and Poisson
% (lambda_mn = lambda_nm) cases. The eigenvalues are computed for each
% Fourier mode, which is part of the exact solutions for W^m and W^n.
%
% For the Markovian Case, this program takes into account the stability of
% the solutions via estimating the range of Fourier modes where each mode
% of the solutions W^m and W^n are stable. From this, the same program can
% be used for a spectrum of stable eigenvalues. These eigenvalues can be
% incorporated to produce approximate solutions for W^m and W^n.
%
% Input Parameters:
%  1.) lambda_mn -- System failure rate going from State m to State n.
%  2.) lambda_nm -- System failure rate going from State m to State n.
%  3.) a_m -- cyber attack rate in State m.
%  4.) a_n -- cyber attafck rate in State n.
%  5.) r_m -- cyber infected rate in State m.
%  6.) r_n -- cyber infected rate in state n.
%  5.) K -- the magnitude of the maximum Fourier mode number. The span of
%  Fourier modes ranges from -K to K.
%  6.) L -- the magnitude of the maximum Fourier mode number. The span of
%  Fourier modes ranges from -L to L.
%
% Output Parameters:
```

```
% Step 1: Defining input parameters. (Right now, just test for Poisson
% Case)
lambda_mn = 3.5;
lambda_nm = 3.5;
K = 12;
L = 12;
a_m = 2;
a_n = 3;
r_m = 2;
r_n = 1;

%Step 2: Allocating the eigenvalue spectrum
kk = -K:K;
ll = -L:L;

%Prestep: initializing vectors
c1 = zeros(length(kk),length(ll));
c2 = zeros(length(kk),length(ll));
phi =zeros(length(kk),length(ll)); % This is for the Poisson case.

% Initializing for the Markovian case as well as preparing for Theorem 1.
RSquared = zeros(length(kk),length(ll));
phi_kl = zeros(length(kk),length(ll));
varpi_kl = zeros(length(kk),length(ll));

%Allocating for recording unstable eigenvalues and modes
c1_unstable = zeros(length(kk),length(ll));
kk_unstable = zeros(1,length(kk));
ll_unstable = zeros(1,length(kk));
countx = 1; %initializing counter for recording unstable modes.
county = 1;

% This is to keep track of the associate location within the vector
% corresponding to the unstable modes.
unstableIndex = zeros(length(kk),length(ll));

% Step 2: Compute eigenvalues for each mode. If lambda_mn = lambda_nm, then
% all of the eigenvalues are stable since the real part is always
% non-positive (i.e. <= 0). Otherwise, we would need to check the
% conditions based on Theorem 1.
```

```
if lambda_mn ==lambda_nm %Poisson case.
lambda = lambda_mn;
for j = 1:length(kk)
for s=1:length(ll)
phi(j,s) = sqrt(lambda^2 - (kk(j)*((a_n - a_m)/2)+ll(s)*((r_n-r_m)/2)^2));
c1(j,s) = -lambda + 1i*(kk(j)*((a_m + a_n)/2)+ll(s)*((r_m+r_n)/2)) + phi(j,s);
c2(j,s) = -lambda + 1i*(kk(j)*((a_m + a_n)/2)+ll(s)*((r_m+r_n)/2)) - phi(j,s);
end % end for l loop
end % end for k loop
else %lambda_mn != lambda_nm (Markov case).
for j =1:length(kk)
for s =1:length(ll)
% Step 2a: Computing R^2, phi_k, and varpi_k
RSquared(j,s) = ((lambda_mn + lambda_nm)^2 -(kk(j))^2*(a_n - a_m)^2
-(ll(s)^2*(r_n-r_m)^2))^2 + 4*((kk(j))*(a_n - a_m)*(lambda_mn - lambda_nm)^2
+(ll(s)*(r_n-r_m))*(lambda_mn - lambda_nm))^2;
R(j,s) = sqrt(RSquared(j,s));
phi_kl(j,s) = sqrt((R(j,s) + ((lambda_mn + lambda_nm)^2
-(kk(j))^2*(a_n - a_m)^2-(ll(s))^2*(r_n-r_m)^2)/2));
varpi_kl(j,s) = sqrt((R(j,s) - ((lambda_mn + lambda_nm)^2
-(kk(j))^2*(a_n - a_m)^2-(ll(s))^2*(r_n-r_m)^2)/2));

%Step 2b: Compute eigenvalue spectrum
c1(j,s) = -((lambda_mn + lambda_nm) + 1i*kk(j)*(a_m + a_n)
+1i*ll(s)*(r_m+r_n))/2 + (phi_kl(j,s) + varpi_kl(j,s))/2;
c2(j,s) = -((lambda_mn + lambda_nm) + 1i*kk(j)*(a_m + a_n)
+1i*ll(s)*(r_m+r_n))/2 - (phi_kl(j,s) + varpi_kl(j,s))/2;

%Step 3: Apply Theorem 1. The goal is to perform a check to determine
%whether the eigenvalue falls within the instability region defined in
%Theorem 1. If it does, then the eigenvalue, Fourier mode, and location
%within each vector is recorded.
dist = (real(c1(j,s) + ((lambda_mn + lambda_nm)/2)^2 + (imag(c1(j,s))
+kk(j)*(a_m + a_n)/2 +ll(s)*(r_m+r_n)/2)^2));
if (real(c1(j,s)) > 0 && dist <= RSquared(j,s)/4)
c1_unstable(countx,county) = c1(j,s); % Recording unstable eigenvalue
kk_unstable(countx) = kk(j); % Recording corresponding unstable mode.
ll_unstable(county) = ll(s);
end
end
end
```

```
end

% Next, gathering the growth rate data to plot corresponding to each
% Fourier mode.
```

Bibliography

[1] SFlow. (2014) Ddos mitigation hybrid open flow controller. [Online]. Available: http://blog.sflow.com/2014/04/ddos-mitigation-hybrid-openflow.html

[2] D. Ravichandran, P. Pantel, and E. Hovy, "The terascale challenge," in *Proc. KDD Workshop on Mining for and from the Semantic Web (MSW-04)*. Citeseer, 2004, pp. 1–11.

[3] C. Howard. (2011) High-performance computing benefits signal- and data processing in aerospace and defense applications. [Online]. Available: www.militaryaerospace.com/articles/2011/07/high-performance-computing.html

[4] N. Hemsoth. (2016) Exascale timeline pushed to 2023: What's missing in supercomputing. [Online]. Available: www.nextplatform.com/2016/04/27/exascale-timeline-pushed-2023-whats-missing-supercomputing/

[5] B. Schroeder and G. A. Gibson, "A large-scale study of failures in high-performance computing systems," *Dependable and Secure Computing, IEEE Transactions on*, vol. 7, no. 4, pp. 337–350, 2010.

BIBLIOGRAPHY

[6] J. Jackson. (2012) Supercomputers face growing resilience problems. [Online]. Available: http://www.computerworld.com/article/2493336/computer-hardware/supercomputers-face-growing-resilience-problems.html

[7] N. DeBardeleben, J. Laros, J. Daly, S. Scott, C. Engelmann, and B. Harrod, "High-end computing resilience: Analysis of issues facing the hec community and path-forward for research and development," *Whitepaper, Dec*, 2009.

[8] A. D. Clark, L. M. Tellez, S. Besse, and J. M. Absher, "Dynamic prediction and estimation of intentional failures in hpcs," in *IEEE/ACM International Conference on Advances in Social Networks Analysis and Mining*. IEEE/ACM, 2016.

[9] D. Quintero, K. Bosworth, P. Chaudhary, R. G. da Silva, B. Ha, J. Higino, M.-E. Kahle, T. Kamenoue, J. Pearson, M. M. Perez *et al.*, *IBM Power Systems 775 for AIX and Linux HPC solution*. IBM Redbooks, 2014.

[10] J. V. Neumann, "Probabilistic logics and the synthesis of reliable organisms from unreliable components," *Automata Studies*, vol. 34, pp. 43–98, 1956.

[11] J. Gray, "Why do computers stop and what can be done about it?" in *Symposium on reliability in distributed software and database systems*. Los Angeles, CA, USA, 1986, pp. 3–12.

[12] J. Gray, "A census of tandem system availability between 1985 and 1990," *Reliability, IEEE Transactions on*, vol. 39, no. 4, pp. 409–418, 1990.

BIBLIOGRAPHY

[13] M. Kalyanakrishnam, Z. Kalbarczyk, and R. Iyer, "Failure data analysis of a lan of windows nt based computers," in *Proceedings of the 18th IEEE Symposium on Reliable Distributed Systems.* IEEE, 1999, pp. 178–187.

[14] I. Lee and R. K. Iyer, "Software dependability in the tandem guardian system," *Software Engineering, IEEE Transactions on*, vol. 21, no. 5, pp. 455–467, 1995.

[15] D. Oppenheimer, A. Ganapathi, and D. A. Patterson, "Why do internet services fail, and what can be done about it?" in *USENIX symposium on internet technologies and systems*, vol. 67. Seattle, WA, 2003.

[16] B. Schroeder and G. A. Gibson, "Understanding failures in petascale computers," in *Journal of Physics: Conference Series*, vol. 78, no. 1. IOP Publishing, 2007, pp. 12–22.

[17] J. Xu, Z. Kalbarczyk, and R. K. Iyer, "Networked windows nt system field failure data analysis," in *Dependable Computing, 1999. Proceedings. 1999 Pacific Rim International Symposium on.* IEEE, 1999, pp. 178–185.

[18] W. Kermack and A. McKendrick, "Contributions to the mathematical theory of epidemicsi," in *Proceedings of the Royal Society of London, Series A.*, vol. 115, no. 5, 1927.

[19] W. Kermack and A. McKendrick, "Contriburions to the mathematical theory of

endemics-ii. the problem of endemicity," in *Proceedings of the Royal Society of London, Series A.*

[20] W.Kermack and A. McKendrick, "Contributions to the mathematical theory of epidemicsiii. further studies of the problem of endemicity," vol. 141, no. 843, 1933, pp. 94–122.

[21] M. E. J. Newman, S. Forrest, and J. Balthrop, "Email networks and the spread of computer viruses," *Physical Review E*, vol. 66, no. 3, p. 035101, 2002.

[22] J. Kim, S. Radhakrishnan, and J. Jang, "Cost optimization in sis model of worm infection," *ETRI journal*, vol. 28, no. 5, pp. 692–695, 2006.

[23] B. K. Mishra and S. K. Pandey, "Dynamic model of worm propagation in computer network," *Applied Mathematical Modelling*, vol. 38, no. 7, pp. 2173–2179, 2014.

[24] C. Zhang, Y. Zhao, and Y. Wu, "An impulse dynamic model for computer worms," in *Abstract and Applied Analysis*, vol. 2013. Hindawi Publishing Corporation, 2013.

[25] W. Fan and K. Yeung, "Virus propagation modeling in facebook," in *The Influence of Technology on Social Network Analysis and Mining.* Springer, 2013, pp. 185–199.

[26] P. Wang, M. C. González, R. Menezes, and A. Barabási, "Understanding the

spread of malicious mobile-phone programs and their damage potential," *International journal of information security*, vol. 12, no. 5, pp. 383–392, 2013.

[27] T. M. Chen, "Propagation modeling of active p2p worms based on ternary matrix," *Journal of Network and Computer Applications*, vol. 36, 2013.

[28] E. Koutsoupias and C. Papadimitriou, "Worst-case equilibria," *Computer science review*, vol. 3, no. 2, pp. 65–69, 2009.

[29] G. Faissol and B. Gallagher, "The price of anarchy and malice: A game theoretic study of targeted failures in hpc systems," *Lawrence Livermore National Laboratory (Technical Report)*, 2014.

[30] N. Nisan, "Algorithms for selfish agents," in *Annual Symposium on Theoretical Aspects of Computer Science*. Springer, 1999, pp. 1–15.

[31] A. D. Clark, "A theoretical representation of the effects of targeted failures in hpc systems," in *Handbook of Research on Next-Generation High Performance Computing*. IGI Global, 2016.

[32] L. A. Pritchett-Sheats, "Evaluation of the cmle row constant model," *Los Alamos National Laboratory (Technical Report)*, 2013.

[33] S. Aalto and W. R. W. Scheinhardt, "Tandem fluid queues fed by homogeneous on–off sources," *Operations Research Letters*, vol. 27, no. 2, pp. 73–82, 2000.

[34] Q. Ren and H. Kobayashi, "Transient solutions for the buffer behavior in statistical multiplexing," *Performance evaluation*, vol. 23, no. 1, pp. 65–87, 1995.

[35] T. Tanaka, O. Hashida, and Y. Takahashi, "Transient analysis of fluid model for atm statistical multiplexer," *Performance evaluation*, vol. 23, no. 2, pp. 145–162, 1995.

[36] B. Sericola, "Transient analysis of stochastic fluid models," *Performance evaluation*, vol. 32, no. 4, pp. 245–263, 1998.

[37] P. Parthasarathy and K. V. Vijayashree, "A fluid queue fed by an on-off source," in *IEEE Annual INDICON*. IEEE, 2005, pp. 396–398.

[38] D. Anick, D. Mitra, and M. M. Sondhi, "Stochastic theory of a data-handling system with multiple sources," *Bell Labs Technical Journal*, vol. 61, no. 8, pp. 1871–1894, 1982.

[39] R. Gaeta, M. Gribaudo, D. Manini, and M. Sereno, "Analysis of resource transfers in peer-to-peer file sharing applications using fluid models," *Performance Evaluation*, vol. 63, no. 3, pp. 149–174, 2006.

[40] G. L. Jones, P. G. Harrison, U. U. Harder, and T. Field, "Fluid queue models of battery life," in *Modeling, Analysis & Simulation of Computer and Telecommunication Systems (MASCOTS), 2011 IEEE 19th International Symposium on*. IEEE, 2011, pp. 278–285.

BIBLIOGRAPHY

[41] N. G. Bean and M. M. O'Reilly, "A stochastic two-dimensional fluid model," *Stochastic Models*, vol. 29, no. 1, pp. 31–63, 2013.

[42] T. Moscibroda, S. Schmid, and R. Wattenhofer, "When selfish meets evil: Byzantine players in a virus inoculation game," in *Proceedings of the twenty-fifth annual ACM symposium on Principles of distributed computing*. ACM, 2006, pp. 35–44.

Vita

Ning Liu was born on July 20, 1989 in Dancheng, Henan, China. He studied at Renmin University of China specializing in Human Resource Management where he received his Bachelors degree in Management in 2012. However, he was very interested in Mathematics where he furthered his graduate studies in this area in the United States. He received a Master of Science (M.S.) in Mathematics from George Washington University and a Master of Science in Engineering (M.S.E) specializing in Applied Mathematics and Statistics from Johns Hopkins University. His research interests lie in theoretical and applied Partial Differential Equations (PDEs), Numerical Analysis of Differential Equations. He plans to pursue his PhD to expound on his knowledge in Mathematics.